

# Inference using a composite-likelihood approximation for stochastic metapopulation model of disease spread

Gaël Beaunée<sup>1\*</sup>, Pauline Ezanno<sup>1</sup>, Alain Joly<sup>2</sup>, Pierre Nicolas<sup>3</sup>, Elisabeta Vergu<sup>3</sup>

**1** Oniris, INRAE, BIOEPAR, 44300 Nantes, France

**2** GDS Bretagne, France

**3** Université Paris-Saclay, INRAE, MaIAGE, Jouy-en-Josas, France

✉ These authors contributed equally to this work.

\* gael.beaunee@inrae.fr

## Abstract

Spatio-temporal pathogen spread is most often partially observed at the metapopulation scale. Available data correspond to proxies and are incomplete, censored and heterogeneous. Moreover, representing such biological systems often leads to complex stochastic models. Such complexity together with data characteristics make the analysis of these systems a challenge.

Our objective was to develop a new inference procedure to estimate key parameters of stochastic metapopulation models of animal disease spread from longitudinal and spatial datasets, while accurately accounting for characteristics of census data. We applied our procedure to provide new knowledge on the regional spread of *Mycobacterium avium* subsp. *paratuberculosis* (*Map*), which causes bovine paratuberculosis, a worldwide endemic disease.

*Map* spread between herds through trade movements was modelled with a stochastic mechanistic model. We used comprehensive data from 2005 to 2013 on cattle movements in 12,857 dairy herds in Brittany (western France) and partial data on animal infection status in 2,278 herds sampled over the period 2007 - 2013. Inference was performed using a new criterion based on a Monte-Carlo approximation of a composite likelihood, coupled to a numerical optimization algorithm (Nelder-Mead Simplex-like).

Our criterion showed a clear superiority to alternative ones in identifying the right parameter values, as assessed by an empirical identifiability on simulated data. Point estimates and profile likelihoods highlighted that a very large proportion ( $> 0.80$ ) of the dairy cattle herds were infected in 2005 with a low infection prevalence on average. We found a moderate and stable risk of purchasing infected cattle from outside the metapopulation (0.14). We confirmed the low average sensitivity of the diagnostic test (0.21).

Our inference procedure could easily be applied to other spatio-temporal infection dynamics, especially for long-lasting endemic diseases. It is of particular interest when ABC-like inference methods fail due to difficulties in defining relevant summary statistics.

## Author summary

# Introduction

To better understand endemic pathogen spread and identify appropriate and targeted control measures, it is necessary to account for interactions occurring between the farm and the regional scales. Indeed, farms are not isolated populations. Especially, movements of animals connect close or distant farms, and represent one of the major transmission routes at large scale [1, 2]. Then, as a result of the well-known rescue effect, pathogen spread occurring due to between-herd contacts may induce infection persistence at large scale while fadeout occurs locally [3]. Furthermore, the diversity of cattle farming systems and local specificities of herd management (e.g. herd size, renewal rate, contact structure) also influence pathogen spread [4, 5]. Each herd has its own demography, which influences the risk of acquiring an infectious disease, the severity and duration of outbreaks within the herd, and the risk of transmitting pathogens to other herds. Factors such as herd size [6], renewal practices [7], within-herd contact structure [8, 9], biosecurity practices [10], and geographical location [11] have been highlighted as largely influencing pathogen spread. Hence, a detailed representation of both the within-population demographic processes (with heterogeneity in herd management among herds) and the epidemiological processes is needed to ensure simulations being realistic enough for tackling practical issues.

However, this gives rise to an increase in model complexity, and thus also in the number of parameters involved and which have to be accurately specified to ensure robust predictions. In managed populations (e.g. in livestock), high resolution data (such as the European databases recording comprehensively cattle movements [12]) are available. This allows a fine grain calibration of demographic processes and to adequately represent population dynamics [13, 14]. Conversely, there is a paucity of available epidemic data, and epidemic dynamics are mostly observed as punctual data points. In addition to being incomplete (data are available for only part of the population), epidemic data generally correspond to proxies, processes being only partially observed. Key events of the infection processes are not observed. For example, if the status of an animal can be known at specific time points (e.g. test dates), the moment when it has changed is not observed. In addition, the difficulty of accurately calibrating a complex model is reinforced by the uncertainty of observations as associated with the imperfect sensitivity of diagnostic tests and more generally infection detection issues.

There is a need for innovative methods to reconcile complex mechanistic models with sparse and heterogeneous data. On the one hand, both the characteristics of such complex models (which are dynamic, with a large number of variables, and even stochastic) and of available data (which are spatiotemporal, incomplete, censored, and imperfect) prevent from defining the likelihood and, therefore, make it impossible to use classical estimation methods (i.e. maximum likelihood). On the other hand, recent advances in likelihood free methods, such as Approximate Bayesian Computations (ABC) [15, 16], and the increase in performance and availability of computing resources have enabled fitting complex models to large-scale epidemic data [17, 18]. However, building the appropriate summary statistics (i.e. containing enough information to be a discriminating criterion), and thus to use ABC-like methods, remains a challenge when tackling heterogeneous units (such as holdings), each having data of variable accuracy and at variable time steps. In addition, although these methods have the advantage of being simulation-based, they generate of a huge number of particles, even in the case of ABC-SMC (Sequential Monte Carlo) [16] which is one of the most effective.

Bovine paratuberculosis, also known as Johne's disease, is a relevant example of an enzootic disease distributed worldwide [19], inducing large economic losses and management issues to farmers [20–22], and for which heterogeneous and sparse epidemiological data are available at farm scale thank to surveys implemented by

animal health services in some areas. There is a need for more robust predictions of the spatio-temporal spread of the causative agent of this chronic inflammatory bowel disease, *Mycobacterium avium* subsp. *paratuberculosis* (*Map*), in order to assess and compare the range of possible control options currently available and to identify the most relevant ones. Many different models have been proposed to predict *Map* spread at farm scale [23], only one focusing on the regional scale [13] to tackle the issue of implementing targeted and adapted control strategies [24]. Because of the characteristics of the pathogen, the associated disease, and the host population, and despite an effort to render such models as parsimonious as possible, these models are quite complex and suffer from parameter uncertainty, especially as regards *Map* transmission, diagnostic test sensitivity, and knowledge about current prevalence at both animal and farm scales.

The objective of this work is twofold. The first objective is to reconcile complex mechanistic epidemiological models and sparse and heterogeneous observed data by developing an alternative approach to the ABC methods to provide an appropriate method when summary statistics are difficult to define, and allowing to better account for unsampled herds in the infection dynamics and to more accurately account for the characteristics of census data for animals tested as positive. The second objective is to gain new knowledge on *Map* spread at a regional scale by estimating the key parameters of a metapopulation epidemiological model from longitudinal and spatial data collected in Brittany (Western France). To the best of our knowledge, this is the first time such an issue is tackled using this type of data. We propose here a new use of these data, taking into account their specific characteristics (scattered, uncomplete, ...) to infer unobservable parameters.

To achieve our objectives, (i) we updated an existing epidemiological model of the regional *Map* spread, (ii) we defined an relevant criterion and an appropriate estimation procedure, (iii) we assessed through simulations the accuracy (closeness to the true value) and precision (variability) of the proposed method, and (iv) we applied our method on real serological survey data to infer seven parameters of the regional epidemiological model of *Map* spread among cattle farms.

## Materials and methods

### Epidemiological data

Among the 18 french administrative regions, Brittany has the highest dairy production and accounted for 22.6% of the total milk volume produced in 2018 in France (source: DRAAF Bretagne). Animal health services (GDS Bretagne) collect data on paratuberculosis in Brittany since the early 2000s using individual serological tests (ELISA) of very high specificity but low and, in fact, relatively unknown sensitivity. Most of these tests take place in punctual screenings that encompass, when possible, all animals that are at least two-year old in the herd. These herd-level screenings can follow the detection of an infected animal (typically after observing clinical signs of the disease or after the positive result of a diagnostic test prescribed for trade), or they can be carried out in the context of a certification program implying regular tests. Although sampling was thus not totally random, we considered here the data as containing unbiased information on herd-level prevalence at heterogeneous points in space and time.

GDS records, which contained the result of each individual test along with precise identification of the animal, were processed to build a high quality dataset of measures of prevalence aggregated at herd level over a 7-year period spanning from 2007 to 2013. For this purpose, tests made on females at least two-year old were grouped into "screening events" consisting of all the tests made in a window of four weeks. The date of the screening event was set as the day with the largest number of tests. Some

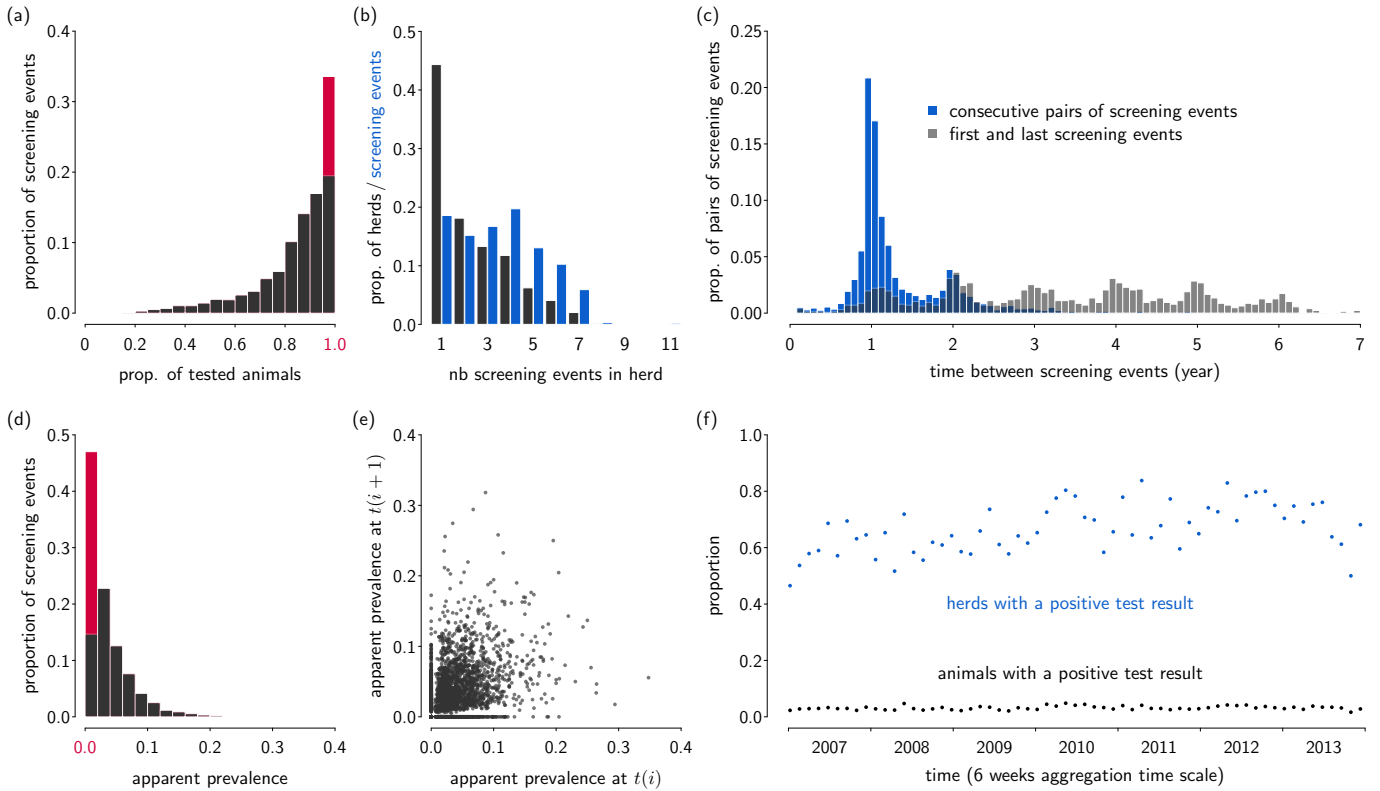


**Fig 1. Overview of the serological data (5,434 selected screening events) available for monitored herds in Brittany (western France) between 2007 and 2013.** Panels of top row describe the testing scheme: (a) proportion of animals of more than two years in the herd tested per screening event; (b) number of screening events in herd for each herd (black) or for each screening event (blue); (c) time between pairs of screening events in a same herd (consecutive screening events in blue, first and last screening events in gray), seasonal pattern, due to higher number screening events in winter. Panels of bottom row describe the results of the serological tests: (d) apparent prevalence among all screening events; (e) comparison of apparent prevalence of two consecutive screening events; (f) apparent prevalence over time: proportion of test-positive animals in tested herds (*i.e.* average prevalence, in black) and of herds with at least one test-positive animal (blue).

screening events were discarded, either because herds belonged to holdings not included in the metapopulation model built on available animal movement data (see below) or because they covered less than 30 animals and 50% of the herd (a minimum of 10 animals was imposed in all cases). This led to a dataset of 5,434 screening events distributed in 2,278 herds with an average proportion of animals in the herd tested per screening event of 85.3% (Fig 1a). Most of the screening events (81.4%) belonged to series of 2 or more for a same herd (Fig 1b). Typical time between consecutive screening events in the same herd was 1 year, with up to 7 years between the first and the last screening event (Fig 1c).

Results of the serological tests established an average apparent prevalence as low as 3.2%, but with at least one positive test in as much as 67% of the screening events (Fig 1d). Apparent prevalence measured at consecutive screening events displayed a mild, but statistically significant, level of correlation (Pearson's  $r=0.39$ ,  $p\text{-value} < 2.2e - 16$ , Fig 1e). Plots of apparent prevalence over time did not reveal any clear trend of temporal evolution (Fig 1f). We refer below to these serological results as the observed epidemiological trajectory. From it, we propose to draw inference on the true

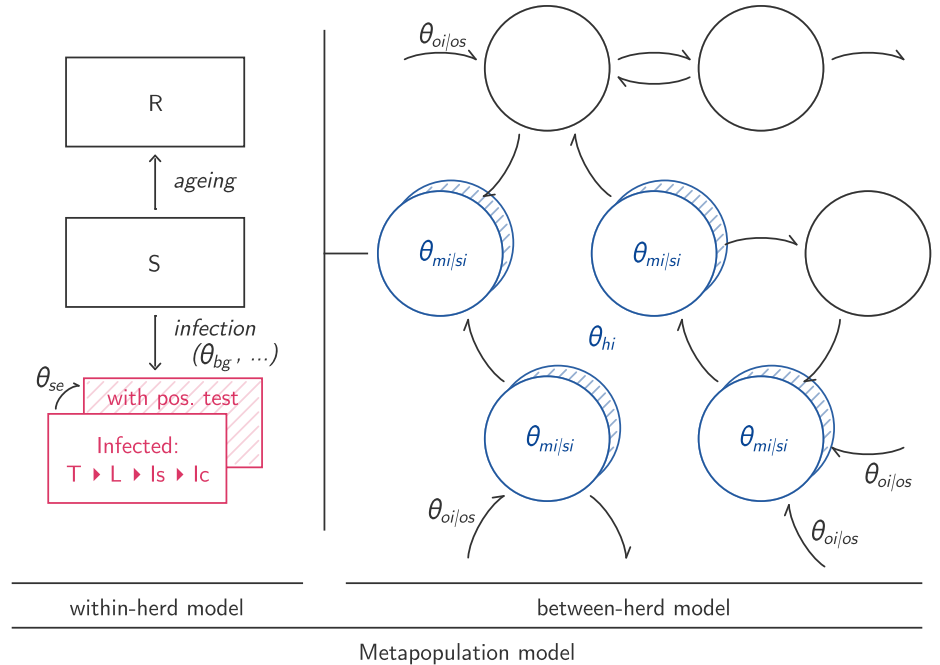


**Fig 2. Conceptual model of Map spread within and between herds.** The left panels gives a simplified view of the within-herd model;  $S$ ,  $R$ ,  $T$ ,  $L$ ,  $Is$ , and  $Ic$  are the six main compartments of the within-herd model. The right panel corresponds to the between-herd model. Curved arrows represent animal movements between herds, herds in blue are infected at the onset of the simulation. In both panels, compartments with hatched line correspond to animals with a positive test result. Definitions of the parameters are given in Table 1.

(unobserved) prevalence and on within-herd transmission based on comparison with the stochastic outcomes of a simulation model.

## Simulation model

The regional spread of Map was simulated using a stochastic metapopulation model adapted from [13,24] that accounts for within-farm and between-farm dynamics. The main characteristics of this model which encompassed here 12,857 farms and the modifications made for this study are described below.

### Within-herd model

Within-herd transmission of Map is represented by a stochastic compartmental model simulated with a discrete time step of one week. The compartments, illustrated in the left panel of Fig 2, distinguish six mutually exclusive classes of animals: young animals susceptible to infection ( $S$ ); older animals (after one year) no longer susceptible ( $R$ ); transient shedders after infection ( $T$ ); latently infected but not infectious ( $L$ ); moderately infectious ( $Is$ ); highly infectious and clinically affected ( $Ic$ ).

Transmission is modelled as occurring through five routes: (i) vertically *in utero*, (ii and iii) horizontally through the ingestion of contaminated colostrum or milk, and (iv and v) indirectly via a contaminated local environment (contaminated by shedding calves) or with the general environment of the farm (contaminated by all shedders). Animals in states  $T$ ,  $Is$  and  $Ic$  shed *Map* in their faeces, and thus contaminate the farm

environment.  $L$  corresponds to a state between  $T$  and  $Is$  in which animals are barely detected as shedders and their shedding is thus neglected [25,26]. Adult infection (after one year of age) is possible [27,28] but is very rare and is also neglected.

Mortality and culling are modelled as stochastic processes whose rates are calibrated specifically for each herd. Compared to [13,24], the model incorporates also a new type of compartment to account for the premature culling of animals detected as positive by serological tests. Namely, each of the existing compartments is split into two sub-compartments that distinguish animals tested positive from untested animals or animals tested negative.

Screening events are simulated at points in space (herds) and time matching the observed epidemiological trajectory. For each screening event, a number of animals given by the proportion of tested animals are randomly selected (among animals of two years and more in the considered herd). The result of each individual serological test is then drawn as the outcome of a Bernoulli trial with probability of success  $\theta_{se}$  if the selected animal is infected (*i.e.* in compartment  $T$ ,  $L$ ,  $Is$  or  $Ic$ ) and is negative for a non-infected animal, assuming a perfect specificity of the test. After a positive test, the average time before culling was set to 24 weeks (as calibrated on real data).

### Between-herd model

Animal movements between herds are implemented deterministically to reproduce the date, origin, destination, and age of actually exchanged animals (see data from cattle tracing records below). The compartment of each exchanged animal is randomly selected according to the distribution of the population in the source herd (excepted for animals in compartment  $Ic$  which are not allowed to move).

This previously published regional model was modified to allow fixing, using dedicated parameters, the probability of purchasing an infected animal from outside the metapopulation. When such an infected animal is purchased, its precise compartment ( $T$ ,  $L$ , or  $Is$ ) is drawn randomly according to the distribution of infected animals in the whole metapopulation.

### Animal movements data

Animal movements were extracted from the French cattle identification database. This database records the life history of each animal from birth to death, including its stays in different types of holdings (*i.e.* farms, markets, and assembling centers). The cattle trade network was simplified down to farm-to-farm movements, neglecting short sojourns of animals in other types of holdings which are not expected to cause new *Map* infections.

Only movements of females of dairy and crossed breeds were considered since French dairy cattle is composed almost exclusively of females, with breeding based on artificial insemination. Fattening activities involving other breeds that are most often conducted in a different building or area of the farm were neglected, and thus we consider each farm as a single herd. Herds with less than 15 dairy females in total or 5 dairy females over two years old, were not included in the network, as these farms are unlikely to represent dairy production units.

Over the 9-year period considered in the simulation (from 2005 to 2013), the resulting metapopulation encompassed 12,857 farms, involved 919,304 animal movements, among which 24.4% were between farms belonging to the metapopulation, 28.8% from external holdings and 46.8% to external holdings.

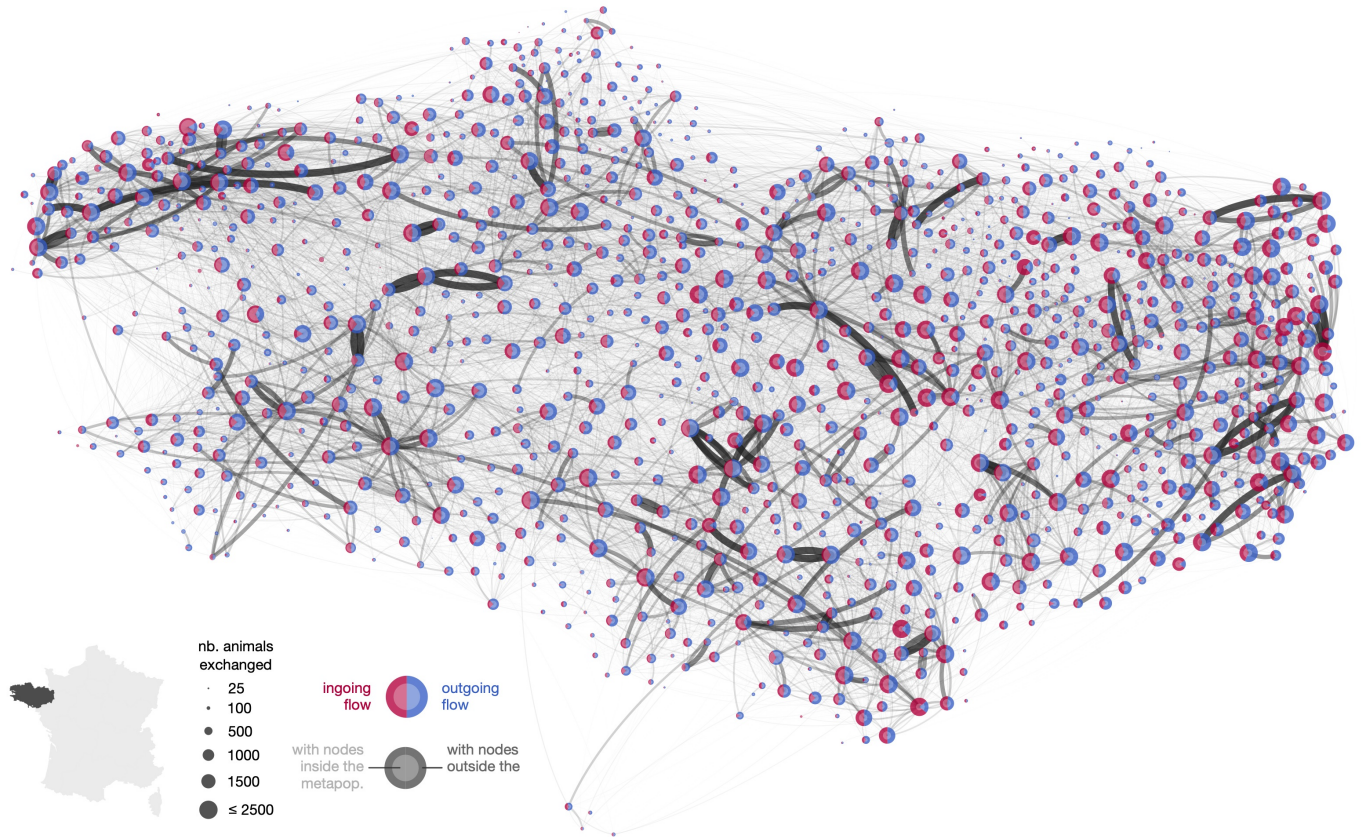


**Fig 3. Cattle trade network between dairy herds located in Brittany (western France) for the period 2005-2013.** Data has been aggregated at the commune level for this representation. Each commune is represented on the map by a disc whose size reflects the total number of exchanged animals. Exchanges between communes are represented by curved lines with thickness proportional to the number of animals exchanged over the period. Each disc is divided in two parts according to the ingoing flow (red) and the outgoing flow (blue), which are themselves split in an inner part corresponding to exchanges with nodes inside the metapopulation, and an outer part corresponding to exchanges with nodes outside the metapopulation.

## Inference method

### Parameter space

Table 1 gives the meaning and allowed range of parameter values for the seven key parameters of the epidemiological model (Fig. 2) which are estimated. The set of these seven parameters is denoted  $\theta = (\theta_{hi}, \theta_{mi}, \theta_{si}, \theta_{oi}, \theta_{od}, \theta_{bg}, \theta_{se})$ . Of note, parameters  $\theta_{mi}$  and  $\theta_{si}$  are those of a normal distribution whose support is truncated to  $(0.0, 0.9)$  to describe the actual initial within-herd prevalence in infected herds. When helpful for interpretation, we report the parameters of the corresponding truncated normal distribution, denoted  $\theta_{mit}$  and  $\theta_{sit}$ .

### Approximate composite likelihood

The whole observed epidemiological trajectory is denoted  $y$ . It consists of the number of positive and negative tests, respectively denoted  $y_{i,j,+}$  and  $y_{i,j,-}$  ( $y_{i,j,\cdot} = y_{i,j,+} + y_{i,j,-}$ ), for each herd  $i$  and screening event  $j$ . Given  $\theta$ , the simulation algorithm allows to

**Table 1. Definition of the seven parameters of the epidemiological model to be estimated.**

Model component and parameter definition	Notation <sup>a</sup>	Min <sup>b</sup>	Max <sup>c</sup>
Initial distribution of infected herds in the metapopulation in 2005			
Proportion of infected herds	$\theta_{hi}$	0.0	1.0
Distribution of within-herd prevalence in infected herds			
Mean of non-truncated Gaussian distribution	$\theta_{mi}$	-1.0	1.0
Standard deviation of non-truncated Gaussian distribution	$\theta_{si}$	0.0	1.0
Mean and standard deviation of the corresponding truncated distribution	$\theta_{mi^t}, \theta_{si^t}$		
Probability of purchasing infected cattle from outside the metapopulation			
Initial probability	$\theta_{oi}$	0.0	1.0
Change over the whole period	$\theta_{od}$	-1.0	1.0
Within-herd transmission through the general environment of the farm			
Coefficient governing transmission rate (log10 scale)	$\theta_{bg}$	-8.0	-4.0
Diagnostic test			
Sensitivity	$\theta_{se}$	0.0	1.0

<sup>a</sup>  $\theta_{mi^t}$  and  $\theta_{si^t}$  are deduced from  $\theta_{mi}$  and  $\theta_{si}$  and thus do not belong to the list of seven free parameters. <sup>b</sup> and <sup>c</sup> gives endpoints of open intervals for the seven estimated parameters and of the allowed range for the within-herd prevalence in infected herds (*i.e.* support of truncation for the Gaussian distribution).

generate random trajectories consisting not only of the positive/negative outcomes of the tests, denoted  $\tilde{y}$ , but also of variables that were not directly observed such as the exact number of infected/non infected animals, denoted  $\tilde{x}$ .

Inference proceeds by optimization over the parameter space of an objective function that compare a given observed trajectory  $y$  to a set of  $K$  trajectories simulated with parameters  $\theta$ . Evaluation of the objective function is necessarily noisy since it depends on a simulated sample of  $K$  random trajectories, denoted  $(\tilde{x}^{(k)}, \tilde{y}^{(k)})_{k=1\dots K}$ . The function that was finally retained is built as the logarithm of a conditional composite likelihood (CC), denoted  $\ell_{CC}(\theta; y)$ , whose terms are approximated using the  $K$  simulated trajectories. The approximation will be referred to as  $\tilde{\ell}_{CC}^K(\theta; y)$  for its noisy evaluation, and  $\ell_{CC}^K(\theta; y)$  for its expected value. The conditional composite likelihood accounts for a first-order Markov dependency between observed values from a same herd. It writes as

$$\ell_{CC}(\theta; y) = \sum_i \left[ \log \pi(y_{i,1} | \theta) + \sum_{j>1} \log \pi(y_{i,j} | y_{i,j-1}, \theta) \right], \quad (1)$$

and its approximation writes

$$\tilde{\ell}_{CC}^K(\theta; y) = \sum_i \left[ \log \tilde{\pi}_K(y_{i,1} | \theta) + \sum_{j>1} \log \tilde{\pi}_K(y_{i,j} | y_{i,j-1}, \theta) \right], \quad (2)$$

where  $\pi(\cdot | \theta)$  denotes densities under the exact model and  $\tilde{\pi}_K(\cdot | \theta)$  denotes their approximations.

The objective function  $\ell_{CC}(\theta; y)$  is a composite likelihood in that it is written as a likelihood but it does not account for all the dependencies of the true stochastic model. Further neglecting dependencies in the formulation of the composite likelihood, we also considered optimizing a marginal composite likelihood (MC),

$$\ell_{MC}(\theta; y) = \sum_{i,j} \log \pi(y_{i,i} | \theta), \quad (3)$$



whose approximation writes

$$\tilde{\ell}_{MC}^K(\theta; y) = \sum_{i,j} \log \tilde{\pi}_K(y_{i,j}|\theta). \quad (4)$$

The  $\tilde{\pi}_K(y_{i,j}|\theta)$ 's are obtained by Monte-Carlo integration as the marginal density of  $y_{i,j}$  under a simplified binomial model for the observed test results  $y_{i,j}$  given the unobserved proportion of infected animals  $x_{i,j,+}/x_{i,j,\cdot}$  and the sensitivity of the diagnostic test  $\theta_{se}$ . Denoting  $\tilde{\psi}_{i,j}^{(k)}$  the corresponding expected proportion of positive tests,

$$\tilde{\psi}_{i,j}^{(k)} = \theta_{se} \frac{\tilde{x}_{i,j-1,+}^{(k)}}{\tilde{x}_{i,j-1,\cdot}^{(k)}}, \quad (5)$$

we write

$$\tilde{\pi}_K(y_{i,j}|\theta) \propto \frac{1}{K} \sum_{k=1}^K \left( \tilde{\psi}_{i,j}^{(k)} \right)^{y_{i,j,+}} \left( 1 - \tilde{\psi}_{i,j}^{(k)} \right)^{y_{i,j,-}}, \quad (6)$$

where the proportionality relationships accounts for a binomial term not needed when comparing composite likelihoods since it depends only on  $y_{i,j}$  and contributes as a same additive constant into  $\tilde{\ell}_{CC}^K(\theta; y)$  and  $\tilde{\ell}_{MC}^K(\theta; y)$ . The same approach is used on the joint density  $(y_{i,j-1}, y_{i,j})$  to obtain the first-order Markov terms in  $\ell_{CC}^K(\theta; y)$  as

$$\tilde{\pi}_K(y_{i,j}|y_{i,j-1}, \theta) = \frac{\tilde{\pi}_K(y_{i,j-1}, y_{i,j}|\theta)}{\tilde{\pi}_K(y_{i,j-1}|\theta)}, \quad (7)$$

with

$$\begin{aligned} & \tilde{\pi}_K(y_{i,j-1}, y_{i,j}|\theta) \\ & \propto \frac{1}{K} \sum_{k=1}^K \left( \tilde{\psi}_{i,j-1}^{(k)} \right)^{y_{i,j-1,+}} \left( 1 - \tilde{\psi}_{i,j-1}^{(k)} \right)^{y_{i,j-1,-}} \left( \tilde{\psi}_{i,j}^{(k)} \right)^{y_{i,j,+}} \left( 1 - \tilde{\psi}_{i,j}^{(k)} \right)^{y_{i,j,-}}. \end{aligned} \quad (8)$$

Eq. 6 would give  $\tilde{\pi}_K(y_{i,j}|\theta) = 0$  when  $y_{i,j,+} > 0$  but  $\tilde{x}_{i,j,+}^{(k)} = 0$  for all  $k = 1 \dots K$ . To obtain a strictly positive value also in these rare cases, the value of  $\tilde{\pi}_K(y_{i,j}|\theta)$  was taken as

$$\tilde{\epsilon}_K(y_{i,j}|\theta) = \frac{1}{K} \left( \frac{\theta_{se}}{\bar{\tilde{x}}_{i,j,\cdot}} \right)^{y_{i,j,+}} \left( 1 - \frac{\theta_{se}}{\bar{\tilde{x}}_{i,j,\cdot}} \right)^{y_{i,j,-}}, \quad (9)$$

where  $\bar{\tilde{x}}_{i,j,\cdot}$  is the average of  $\tilde{x}_{i,j,\cdot}^{(k)}$  across the  $K$  simulated trajectories. The rationale for the choice of this  $\tilde{\epsilon}_K(y_{i,j}|\theta)$  is to correspond to one infected animal at point  $(i, j)$  in one of the  $K$  simulated trajectory. Similarly,  $\tilde{\pi}_K(y_{i,j}|y_{i,j-1}, \theta)$  could not be computed with Eq. 9 when  $y_{i,j-1,+} > 0$  but  $\tilde{x}_{i,j-1,+}^{(k)} = 0$  for all  $k = 1 \dots K$  and this term was in these rare cases replaced by  $\tilde{\pi}_K(y_{i,j}|\theta)$  computed with Eq. 6.

### Alternative objective functions

Other objective functions were considered in the initial steps of this work but not used for final inference. Three are more particularly mentioned in the results section. The first is the average sum of squared differences between the proportion of positive tests in  $y_{i,j}$  and  $\tilde{y}_{i,j}^{(k)}$  (ASSD), computed as

$$\tilde{f}_{ASSD}^K(\theta; y) = \frac{1}{K} \sum_{k=1}^K \sum_{i,j} \left( \frac{y_{i,j,+}}{y_{i,j,\cdot}} - \frac{\tilde{y}_{i,j,+}^k}{\tilde{y}_{i,j,\cdot}^k} \right)^2. \quad (10)$$

The second is the sum of squared of differences between the average proportion of positive tests in  $y_{i,j}$  and  $\tilde{y}_{i,j}^{(k)}$  (SSDA), computed as

$$\tilde{f}_{SSDA}^K(\theta; y) = \sum_{i,j} \left( \frac{y_{i,j,+}}{y_{i,j,\cdot}} - \frac{1}{K} \sum_{k=1}^K \frac{\tilde{y}_{i,j,+}^k}{\tilde{y}_{i,j,\cdot}^k} \right)^2. \quad (11)$$

The third corresponds to the log-likelihood under a binomial model with independent  $y_{i,j}$ 's (BI), computed as

$$\tilde{\ell}_{BI}^K(\theta; y) = \sum_{i,j} y_{i,j,+} \log \left( \frac{1}{K} \sum_{k=1}^K \frac{\tilde{y}_{i,j,+}^k}{\tilde{y}_{i,j,\cdot}^k} \right) + y_{i,j,-} \log \left( 1 - \frac{1}{K} \sum_{k=1}^K \frac{\tilde{y}_{i,j,+}^k}{\tilde{y}_{i,j,\cdot}^k} \right). \quad (12)$$

The objective functions  $f_{ASSD}^K$  and  $f_{SSDA}^K$  are to be minimized while the objective functions  $\ell_{BI}^K$  is to be maximized. Variations around Eq. 10-12 are possible. In particular, the option of replacing the proportion of positive tests  $\tilde{y}_{i,j,+}^k/\tilde{y}_{i,j,\cdot}^k$  by its expected value (Eq. 5) was considered, and the corresponding objective functions are referred to as  $f_{ASSDe}^K$ ,  $f_{SSDAe}^K$ , and  $\ell_{BIe}^K$ . For  $f_{ASSD}^K$  and  $f_{SSDA}^K$ , reweighing each term  $(i,j)$  of the sum by  $y_{i,j,\cdot}^2$  changes the differences between proportions into differences between counts and led to  $f_{ASSDc}^K$  and  $f_{SSDAc}^K$ .

### Optimization based on Nelder-Mead algorithm

Evaluation of the objective function is computationally expensive due to the size of the simulated system (12,857 farms linked through 919,304 animal movements) and the need for repetitions (Monte Carlo integration with  $K = 100$  in practice).

Nelder-Mead algorithm (also known as Simplex) [29] was chosen among the multitude of optimization algorithms. This algorithm has the advantage of being efficient, straightforward to implement, and derivative-free. To explore a  $I$ -dimensional space the algorithm captures information on the local shape of the objective function by using  $I + 1$  test points (the simplex). Iterations use this information to update the simplex by choosing between reflection, expansion, contraction, and shrink steps. Given the usual formulation of the algorithm as solving a minimization problem, we minimized  $-\ell_{CC}^K(\theta; y)$ . Also, since the algorithm works in  $\mathbb{R}^I$ , to restrain the optimization to the parameter space defined by the minimum and maximum values allowed for each parameter ( $\theta_i \in ]\theta_i^{min}, \theta_i^{max}[$ ), logit transformations were applied (optimization on  $x_i \in ]-\infty, +\infty[$  and  $\theta_i = \theta_i^{min} + (\theta_i^{max} - \theta_i^{min})/(1 + e^{-x_i})$ ).

To cope with stochastic noise in the evaluation of the objective function, the Nelder-Mead algorithm was adapted along the lines proposed by [30]. These adaptations consist of (i) re-evaluation of the objective function at all points of the simplex after a shrink step, (ii) choice of a small amplitude for the shrink step (coefficient of 0.9 instead of the more commonly used value of 0.5), and (iii) restarting several times the algorithm by constructing a fresh simplex with the size of the initial regular simplex, centered on the current best point. When not specified otherwise in the text, such fresh restarts are done every 100 iterations.

Starting from an initial simplex, the output of the algorithm is a sequence of  $(\theta^{(m)})_{m=1,\dots,M}$  whose each element is associated with an evaluation of the objective function,  $\tilde{\ell}_{CC}^K(\theta^{(m)}; y)$ . The  $\tilde{\ell}_{CC}^K(\theta^{(m)}; y)$  are not always increasing due to the adaptations (i) and (iii). The final point estimate  $\hat{\theta}$  was chosen as  $\theta^{(m^*)}$  with  $m^* = \arg \max_m \tilde{\ell}_{CC}^K(\theta^{(m)}; y)$ . An estimate of  $\ell_{CC}^K(\hat{\theta}; y)$ , denoted  $\bar{\ell}_{CC}^K(\hat{\theta}; y)$ , was obtained by averaging 10 independent evaluations of  $\tilde{\ell}_{CC}^K(\hat{\theta}; y)$ .

## From point estimates to confidence intervals using profiles

Use of Nelder-Mead algorithm leads to a point estimate  $\hat{\theta}$  of the parameters in a space of dimension  $I = 7$  and an estimate of the corresponding value of the maximized objective function  $\bar{\ell}_{CC}^K(\hat{\theta}; y)$ . A "profile likelihood" approach served to obtain confidence intervals for each parameter  $i$ . Namely, confidence intervals at level  $\alpha$  are defined for the  $i^{\text{th}}$  parameter as the range of values for  $\theta_i$  which are compatible with a value of the objective function above  $\bar{\ell}_{CC}^K(\hat{\theta}; y) - \tau_\alpha$ . In practice, these intervals are delineated after establishing a profile of  $\max_{\theta_{-i}} \bar{\ell}_{CC}^K((\theta_i, \theta_{-i}); y)$  as a function of  $\theta_i$ , where  $\theta_{-i}$  denotes all the parameters but  $\theta_i$ . This is achieved by fixing  $\theta_i$  to various values and performing maximization with respect to  $\theta_{-i}$  (i.e. in a space of dimension  $I - 1$ ) using Nelder-Mead algorithm. For this purpose, the initial simplex is chosen centered on  $\hat{\theta}_{-i}$  and periodic restarts are deactivated.

Whereas in the classical maximum likelihood inference framework asymptotic results justify the use of quantiles of chi-squared distribution [31], the tolerance threshold  $\tau_\alpha$  for level  $\alpha = 95\%$  needed here to be calibrated by estimation on simulated datasets (see results).

## Results

### Choice of the objective function on simulated datasets

An extensive simulation study was conducted to compare the performances of different candidate objective functions that could be used for inference. This numerical study started by selecting 2,000 scenarios, each corresponding to a distinct value of  $\theta$ . Dispersion of the scenarios and hence coverage of the parameter space was maximized by Latin Hypercube Sampling (LHS), accounting for a constraint on the shape of the within-herd prevalence distribution:  $\Phi_{\theta_{mi}, \theta_{si}}(0) >= 0.1$ , in order to avoid too many similar truncated distribution shapes. For each scenario, the simulation model was used to generate 101 epidemiological trajectories, out of which 1 served as an observed dataset (i.e. playing the role of real data). The other 100 served to compute the terms of the objective function needed to compare any observed data to this particular scenario using any objective function (i.e. playing the role of the simulated data with  $K = 100$  in Eq. 2 and 4). Each simulated observed dataset was then compared to each scenario (2,000  $\times$  2,000 comparisons) using 16 candidate objective functions.

Performance of the 5 main types of objective functions, in terms of ability to identify the scenario that generated the observed data, are reported in Table 2 (see S1 Table for the other candidate objective functions). Objective functions based on approximate composite likelihoods ( $\tilde{\ell}_{MC}^{100}(\theta; y)$  and  $\tilde{\ell}_{CC}^{100}(\theta; y)$ ) were able to identify the correct scenario (among 2,000) for more than 95% of the simulated observed datasets. These functions produced about twice less errors than more traditional objective functions based on the sum of squared deviations from the mean of the 100 simulations ( $\tilde{f}_{SSDA}^{100}$  and  $\tilde{f}_{SSDAc}^{100}$ ) which achieved about 90% of correct scenario identification. Objective functions built as the sum of squared differences between observed data and each of the 100 simulations before averaging the results ( $\tilde{f}_{ASSD}^{100}$  and  $\tilde{f}_{ASSDc}^{100}$ ) obtained dramatically lower performances with only about 2% of correct scenario identification.

Markov transition terms introduced in  $\tilde{\ell}_{CC}^{100}(\theta; y)$  to take into account dependence between consecutive sampling points in the same herd did not produce benefits that could be easily seen Table 2 (in the comparison with  $\tilde{\ell}_{MC}^{100}(\theta; y)$ ). Another perspective for the comparison of  $\tilde{\ell}_{CC}^{100}(\theta; y)$  and  $\tilde{\ell}_{MC}^{100}(\theta; y)$ , is to see these approximate composite likelihoods as regular likelihoods associated with two different models, each one attempting to approach the true distribution of the observed data. A closer

Table 2. Evaluation of candidate objective functions for inference based on a LHS of 2,000 scenarios.

Performance measure <sup>a</sup>	Objective function <sup>b</sup>				
	$\tilde{f}_{ASSD}^{100}$	$\tilde{f}_{SSDA}^{100}$	$\tilde{\ell}_{BI}^{100}$	$\tilde{\ell}_{MC}^{100}$	$\tilde{\ell}_{CC}^{100}$
Rank of $\theta^0$					
first ( <i>i.e.</i> $\theta^* = \theta^0$ )	0.170	0.897	0.754	0.970	0.954
top 5%	0.369	1.00	1.00	1.00	1.00
Error on parameter ( $ \theta^* - \theta^0 / \theta^{\max} - \theta^{\min} $ )					
$\theta_{hi}$	0.285	0.019	0.034	0.001	0.002
$\theta_{mi}$	0.259	0.027	0.072	0.006	0.011
$\theta_{si}$	0.352	0.027	0.069	0.006	0.009
$\theta_{mit}$	0.206	0.017	0.043	0.004	0.006
$\theta_{sit}$	0.278	0.019	0.048	0.004	0.007
$\theta_{oi}$	0.278	0.015	0.040	0.004	0.005
$\theta_{od}$	0.254	0.016	0.039	0.005	0.007
$\theta_{bg}$	0.146	0.008	0.023	0.002	0.003
$\theta_{se}$	0.196	0.012	0.022	0.002	0.003
Error on parameter, after excluding the true scenario ( $ \theta^+ - \theta^0 / \theta^{\max} - \theta^{\min} $ )					
$\theta_{hi}$	0.287	0.157	0.152	0.080	0.085
$\theta_{mi}$	0.262	0.276	0.282	0.246	0.245
$\theta_{si}$	0.358	0.288	0.299	0.257	0.253
$\theta_{mit}$	0.209	0.171	0.173	0.143	0.139
$\theta_{sit}$	0.283	0.211	0.216	0.174	0.170
$\theta_{oi}$	0.281	0.166	0.173	0.148	0.148
$\theta_{od}$	0.258	0.177	0.178	0.175	0.171
$\theta_{bg}$	0.148	0.076	0.084	0.081	0.077
$\theta_{se}$	0.197	0.083	0.082	0.059	0.057

<sup>a</sup> For each performance measure, results reported here are average over 2,000 simulated observed datasets. Notations:  $\theta^0$ , the set of parameters that served to simulate the observed dataset (*i.e.* the “truth”);  $\theta^*$ , the set of parameters that maximized the objective function, and  $\theta^+$ , the set of parameters that maximized the objective function after excluding  $\theta^0$ . <sup>b</sup> Objective functions described in the text, identified by subscript labels: *ASSD*, average sum of squared differences; *SSDA*, sum of squared of differences; *BI*, binomial independent; *MC*, marginal composite likelihood; *CC*, conditional composite likelihood. Gray and light gray backgrounds highlight, respectively, best and second best objective functions with respect to each performance measure.

representation of the true model is thus expected to lead to a higher value of the approximate composite likelihood. From this perspective,  $\tilde{\ell}_{CC}^{100}(\theta; y)$  is clearly better than  $\tilde{\ell}_{MC}^{100}(\theta; y)$  since  $\tilde{\ell}_{CC}^{100}(\theta^0; y)$  was higher than  $\tilde{\ell}_{MC}^{100}(\theta^0; y)$  for 99.55% of the couples  $(\theta^0, y)$  where  $\theta^0$  denotes the parameter values that served to generate  $y$  (S1 Fig). The approximate composite likelihood  $\tilde{\ell}_{CC}^{100}(\theta; y)$  was thus selected as the objective function maximized with respect to  $\theta$  for inference.

### Validation of point estimates on simulated datasets

The estimation procedure based on numerical optimization was evaluated on a set of 20 scenarios selected by a LHS. Here, the number of scenarios was lower than analyzed to choose the objective function due to the computational cost of the optimization, which requires many evaluations of the objective function. In practice, a total of 40 observed

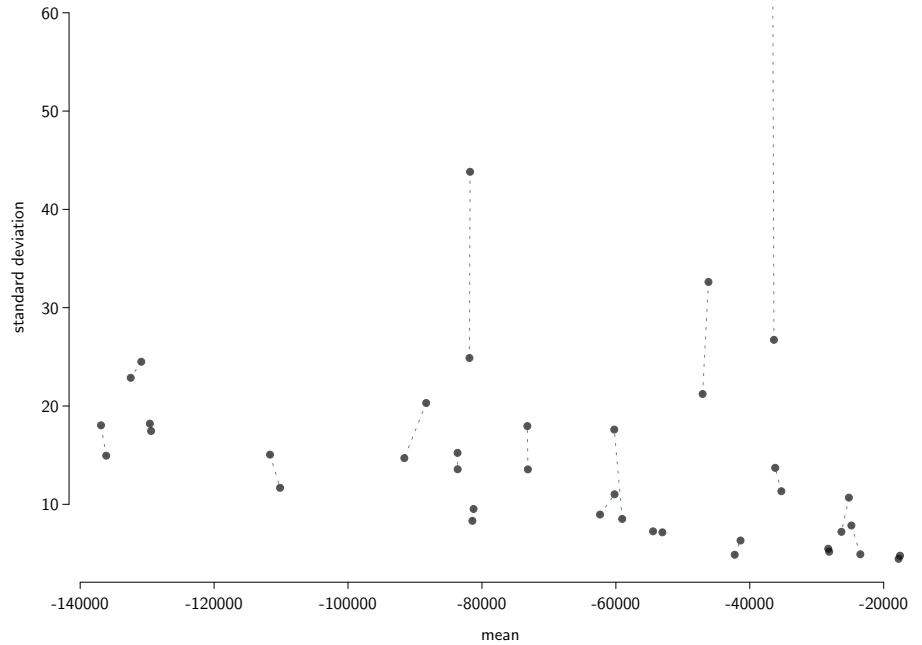


**Fig 4.** Mean and standard deviation of the approximate composite likelihood on simulated observed datasets. For each of the 40 simulated observed dataset  $y$ , the mean (x-axis) and standard deviation (y-axis) of 20 evaluations of  $\tilde{\ell}_{CC}^{100}(\theta^0; y)$  are reported, where  $\theta^0$  is the set of parameters that served to generate  $y$ .

datasets were simulated, with 2 independent simulations for each of the 20 scenarios to unveil variability associated with the randomness of the observed dataset given the parameter values.

These 40 simulated observed datasets from 20 different scenarios covered a wide range of values for the mean and standard deviation of the objective function (the scenarios were constructed on the basis of two LHS, including one for which the parameters of the within-herd prevalence distribution were manually defined). As shown in Fig. 4, the approximate composite log-likelihood  $\tilde{\ell}_{CC}^{100}(\theta^0; y)$  varied across the 20 scenarios by an amplitude of approximately 7-fold in terms of estimated mean (from around -140,000 to -20,000) and more than 10-fold in terms of estimated standard deviation (from around 5 to 60). Not unexpectedly, Fig. 4 shows a trend for a positive correlation between the absolute value of the mean and the standard deviation and some differences between duplicated simulations.

For each dataset, numerical maximization of  $\ell_{CC}^{100}(\theta; y)$  with respect to  $\theta$  lead to a point estimate  $\hat{\theta}$ . Fig. 5 illustrates the behaviour of this numerical optimization on the real data and demonstrates the importance of periodic fresh restarts to minimize the impact of the starting point. Fig. 6 shows the results obtained for the 40 simulated datasets based on 3 fresh restarts (300 iterations). Attesting of the effectiveness of the optimization procedure, point estimates  $\hat{\theta}$  were always such as  $\tilde{\ell}_{CC}^{100}(\hat{\theta}; y)$  is close to  $\tilde{\ell}_{CC}^{100}(\theta^0; y)$  (Fig. 6a). Of note, an ideal optimization procedure is expected to reach a value for  $\tilde{\ell}_{CC}^{100}(\hat{\theta}; y)$  higher than  $\tilde{\ell}_{CC}^{100}(\theta^0; y)$ . This was the case for 26 (65%) of the simulated datasets.

Comparison of point estimates,  $\hat{\theta}$ , with true values of the parameters used to

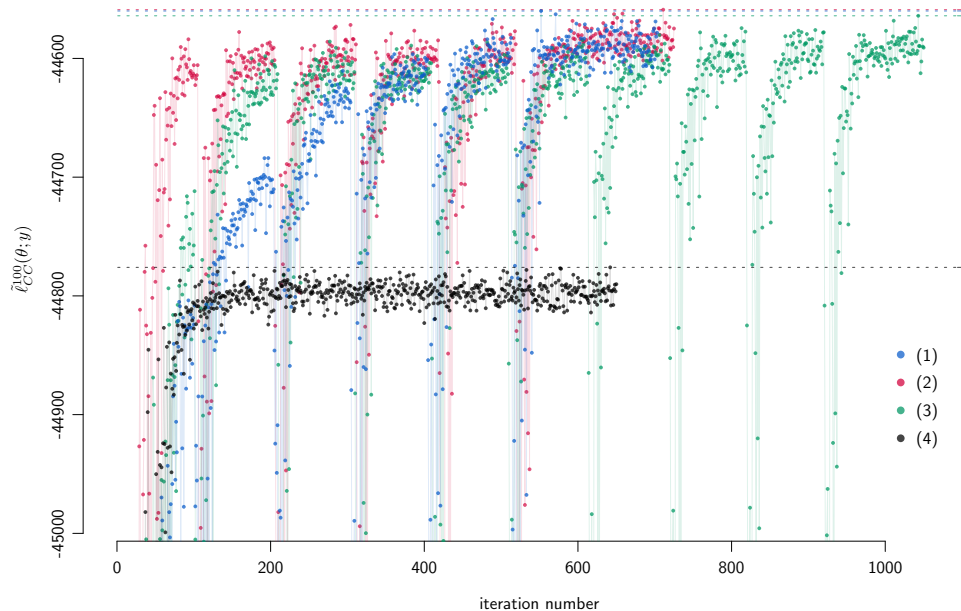


**Fig 5.** Behaviour of the optimization procedure used for parameter estimation. Iterations of the modified Nelder-Mead algorithm are counted in number of evaluations of the approximate composite likelihood  $\hat{\ell}_{CC}^{100}(\theta; y)$  used as objective function. Four trajectories obtained on the real observed dataset from Brittany are represented with different colors. Blue, red, and green trajectories differ by their starting points while the black one corresponds to a trajectory without periodic fresh restarts restoring the initial size of the simplex.

simulate the data,  $\theta^0$ , revealed a good performance of the estimators, as reported in Fig. 6b-h (details in S2 Table). For 4 out of the 7 parameters, the fraction of explained variance ( $R^2$ ) was even higher than 0.9. The 3 parameters that did not reach this threshold were  $\theta_{si}$ ,  $\theta_{od}$ , and  $\theta_{mi}$ , with  $R^2$  respectively of 0.58, 0.64 and 0.84. Two distinct factors could contribute to lower  $R^2$ . The first is genuine statistical uncertainty of point estimates which would translate into a relatively flatter profile of the objective function and larger confidence intervals (see below). This uncertainty could be due to a smaller impact of the parameter on the model outcome or to the possibility of compensation between parameters. In particular, interplay between  $\theta_{mi}$  and  $\theta_{si}$  in the definition of the initial distribution of prevalence in infected herds may pose difficulties for point estimations (S2 Fig). The second factor is sub-optimal numerical maximization of the objective function. Suggesting that sub-optimal maximization plays a role in the lower  $R^2$ , we noticed that for the 3 parameters with  $R^2 < 0.9$  the  $R^2$  could be increased by considering only the datasets for which  $\bar{\ell}_{CC}^{100}(\hat{\theta}; y) > \bar{\ell}_{CC}^{100}(\theta^0; y)$  (see Fig. 6b-h). The effect was particularly strong for  $\theta_{si}$ , for which  $R^2$  raised from 0.58 to 0.90. Of note, the two factors contributing to lower  $R^2$  are not expected to be disconnected since maximization is more difficult when the objective function is not steep compared to the level of noise in its evaluation.

### Calibration of thresholds to build confidence intervals

Confidence intervals are built by delineation of regions in the parameter space that are close, in terms of value of the objective function, to  $\hat{\theta}$  which represents the best set of

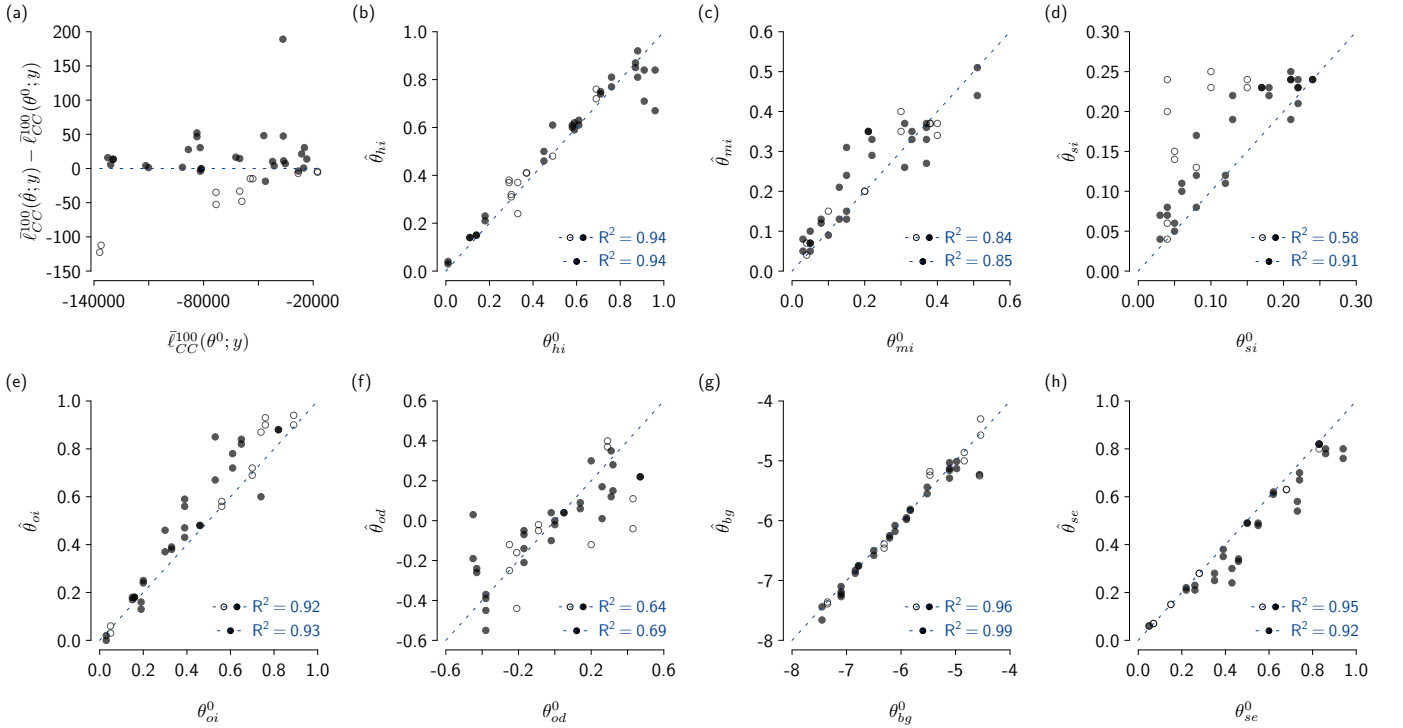


**Fig 6.** Characteristics of point estimates of the parameters on simulated datasets. Results are based on independent point estimations carried out on 40 distinct datasets. (a) Comparison between the value of the approximate composite likelihood  $\bar{\ell}_{CC}^{100}(\hat{\theta}; y)$  evaluated at  $\hat{\theta}$  (point estimate) and  $\theta^0$  (set of parameters used to simulate the observed data). Datasets are represented by black points when  $\bar{\ell}_{CC}^{100}(\hat{\theta}; y) > \bar{\ell}_{CC}^{100}(\theta^0; y)$  or when the difference is not statistically different at the 5% significance level as assessed with a t-test comparing the 10 evaluations of  $\bar{\ell}_{CC}^{100}(\theta; y)$  used to compute  $\bar{\ell}_{CC}^{100}(\theta; y)$  for each  $\theta$ . White points are used otherwise. (b-h) Comparison between  $\hat{\theta}$  and  $\theta^0$  for each of the seven model parameters; same color code as in (a).

parameter values found for the dataset. Under the conditions of the asymptotic theory of maximum likelihood estimation, thresholds  $\tau_\alpha$  that define confidence intervals of one-dimensional parameters are given by the quantiles of the Chi-squared distribution with one-degree of freedom. Boundaries of intervals at  $\alpha = 95\%$  are then located where the value of the log-likelihood drops 1.92 below its maximum. By using an objective function built as an approximate composite log-likelihood, we are not in the conditions of this theory, and we thus conducted a numerical analysis to calibrate the thresholds that could serve to build confidence intervals.

Thresholds corresponding to a target confidence level of 95% were calibrated on the 40 simulated datasets that served to validate point estimates. For each simulated dataset and each parameter  $i$  (out of the 7 model parameters), we examined the distribution of the difference  $\bar{\ell}_{CC}^{100}(\hat{\theta}; y) - \bar{\ell}_{CC}^{100}(\theta_i^0, \hat{\theta}_{-i}; y)$ , where  $\hat{\theta}_{-i}$  is obtained by numerical optimization with  $\theta_i$  held fixed at  $\theta_i^0$ . Based on the histogram aggregating all datasets and all parameters (Fig. 7), the threshold was established at 41.18.

The empirical distribution shown in Fig. 7 is far from a Chi-squared distribution with one-degree of freedom. This was anticipated not only given the use of an objective which is not the genuine log-likelihood of the model that generated the data, but also given noisy evaluation of the objective function and the associated sub-optimal behavior of the numerical optimization. To assess robustness with respect to this last point we examined if the distribution differed when excluding the datasets for which the point

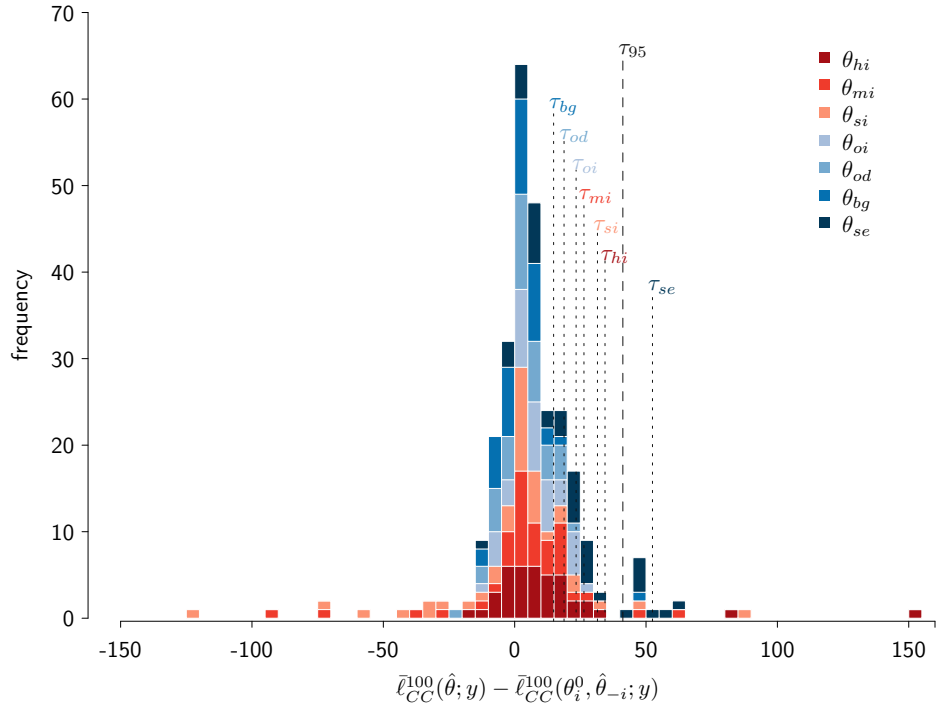


**Fig 7.** Calibration of thresholds to build confidence intervals. Empirical distributions of  $\bar{\ell}_{CC}^{100}(\hat{\theta}; y) - \bar{\ell}_{CC}^{100}(\theta_i^0, \hat{\theta}_{-i}; y)$  are represented along with quantiles at level 95%. Colors distinguish the 7 parameters of the model. Quantiles of the total aggregated distribution and specific of each parameter are reported.

estimate is farther from its optimal value as detected by  $\bar{\ell}_{CC}^{100}(\hat{\theta}; y)$  being significantly below  $\bar{\ell}_{CC}^{100}(\theta^0; y)$  (white points in Fig. 6). No clear impact of these points was observed since the resulting threshold was established at 45.12 (S3 Fig). Importantly, departure from the conditions of the asymptotic theory of maximum likelihood estimation makes that the hypothesis of a common threshold for all parameters may not hold. To cope with this issue, thresholds were also established separately for each parameter (Fig. 7(b)). This confirmed a substantial variability between parameters, with thresholds ranging from 14.83 (for  $\theta_{bg}$ ) to 52.45 (for  $\theta_{se}$ ). For all but  $\theta_{se}$  these parameter-specific thresholds were lower than the global threshold. Their use tends thus to lead to narrower, more optimistic, confidence intervals. To be conservative, the two types of confidence intervals, based on global and parameter-specific thresholds, are reported for real data below.

## Estimation of epidemiological parameters on serological data from Brittany

To circumvent the risk of sub-optimal point estimation due to the difficulty of maximizing the objective function, the results of numerical optimization from three distant starting points were compared and extra iterations of the algorithm were performed (Fig. 5). A first starting point was the center of the parameter space (center of the interval of allowed values for each parameter), a second starting point was based on experts opinion (potentially close to probable values), a third starting point was selected to be distant from expert opinion. After following different paths in the



parameter space (S4 Fig), the three numerical optimization trajectories converged towards similar values of the objective function and of the parameters (Table 3). It is therefore very likely that the region of the parameter space where the objective function is maximum has been correctly identified.

To rule out the possibility of clear discrepancy between the model and the data that would jeopardize the relevance of the estimates, we compared epidemiological trajectories simulated with parameters corresponding to these point estimates to the real data. For this purpose, the distribution of positive tests over time in the observed data was examined both in terms of fraction of herd screening events that reported at least a positive test (Fig. 8a) and in terms of distribution of the fraction of positive tests in screening events (Fig. 8b-e). The simulated trajectories reproduced faithfully these characteristics of the real data.

Point estimates and their associated confidence intervals allow to draw a detailed picture of the status and dynamics of Map spread in Brittany. The key parameter that connects observed and real prevalence of the disease is  $\theta_{se}$ , the sensitivity of the diagnostic test. This sensitivity is estimated at 0.21. A total of 5 parameters characterize the prevalence at the temporal and spatial boundaries of the metapopulation. For the temporal aspect, the initial prevalence is characterized by a very high proportion of initially infected herds ( $\hat{\theta}_{hi} = 0.97$ ) but a relatively low prevalence within these herds (mean  $\hat{\theta}_{mit} = 0.17$  and standard deviation  $\hat{\theta}_{sit} = 0.15$ ). The resulting initial overall prevalence in the metapopulation is 0.16 ( $\hat{\theta}_{hi} \times \hat{\theta}_{mit}$ ). For the spatial aspect, the estimated probability to purchase an infected animal from outside the metapopulation appears to be comparable to this overall prevalence ( $\theta_{oi} = 0.14$ ) and almost constant over time ( $\theta_{od} \approx 0$ ). Finally, the key parameter of the dynamics within the metapopulation (animal movements being given) is  $\theta_{bg}$ , the logarithm of the coefficient governing the within-herd transmission rate through the general environment of the farm. It is estimated to  $-6.80$ .

Confidence intervals associated with each of the parameter estimates were determined by drawing profiles of the objective function and applying the thresholds numerically established on simulated data (Fig 9). Profiles obtained for parameters  $\theta_{hi}$ ,  $\theta_{bg}$ , and  $\theta_{se}$  were highly discriminating, with large differences in the objective function across the range of possible parameter values. Accordingly, confidence intervals (Table 3) established for these parameters are narrower than for the initial distribution of within-herd prevalence ( $\theta_{mi}$  and  $\theta_{si}$ ) and for the probability of purchasing an infected animal from outside the metapopulation ( $\theta_{oi}$  and  $\theta_{od}$ ). The estimations conducted in order to draw the profiles show clear compensation effects between some parameters (S5 Fig). As mentioned above, the parameters of the initial within-herd prevalence distribution ( $\theta_{mi}$  and  $\theta_{si}$ ) evolved together to obtain similar truncated distribution shapes, leading to a relatively flat profile for the objective function near their point estimates. For the probability of purchasing infected cattle from outside the metapopulation ( $\theta_{oi}$  and  $\theta_{od}$ ), we also observed a negative correlation between intercept and slope, with  $\theta_{od} > 0$  when  $\theta_{oi} < \hat{\theta}_{oi}$  and  $\theta_{od} < 0$  when  $\theta_{oi} > \hat{\theta}_{oi}$ .

## Discussion

In this work, we proposed a likelihood free inference procedure to estimate disease spread parameters at a metapopulation level. We defined two new and highly efficient objective functions based on approximate composite likelihoods which identified the correct scenario in more than 95% of the synthetic datasets. The criteria designed correctly deal with the imperfect detection of the infection due to the lack of sensitivity of the diagnostic test and the high proportion of test-negative animals (low prevalence level in the herds). Applying our method to serological observations from a longitudinal

**Table 3. Estimated parameter values on real epidemiological survey data (Brittany, France)**

	Point estimates <sup>a</sup>			Confidence intervals (95%)			
				shared $\tau_{95}$ <sup>b</sup>		param.-sp. $\tau_{95}$ <sup>c</sup>	
	Run 1	Run 2	Run 3	Min	Max	Min	Max
$\theta_{hi}$	0.97	0.97	0.95	0.90	<u>1.00</u>	0.91	<u>1.00</u>
$\theta_{mi}$ ( $\theta_{mit}$ )	-0.42 (0.17)	-0.37 (0.17)	-0.43 (0.18)	<u>-1.00</u>	0.03	<u>-1.00</u>	0.00
$\theta_{si}$ ( $\theta_{sit}$ )	0.35 (0.15)	0.34 (0.14)	0.37 (0.16)	0.07	0.53	0.11	0.51
$\theta_{oi}$	0.14	0.15	0.13	<u>0.00</u>	0.33	0.02	0.29
$\theta_{od}$	-0.01	0.03	0.02	-0.31	0.34	-0.15	0.27
$\theta_{bg}$	-6.80	-6.79	-6.78	-7.00	-6.60	-6.91	-6.71
$\theta_{se}$	0.21	0.21	0.20	0.15	0.29	0.14	0.31
$\bar{\ell}_{CC}^{100}(\hat{\theta}; y)$	-44 580	-44 584	-44 585				

<sup>a</sup> Results are given for three runs of the numerical optimization algorithm. Highest estimated value for the objective function,  $\bar{\ell}_{CC}^{100}(\hat{\theta}; y)$ , was for run 1 (highlighted in gray). <sup>b</sup> and <sup>c</sup> gives endpoints of confidence intervals determined either on the basis of a shared cut-off for all the parameters or of parameter specific cut-offs. Underlined and overlined values indicates boundary of the parameter space. Definitions of the parameters are given in Table 1.

dataset for bovine paratuberculosis in Brittany (western France), we draw a detailed picture of infection herd statuses and of the regional spread of Map.

TBC

## Conclusion

The likelihood-free inference procedure presented in this paper is able to deal with limited data, such as a number of test-positive animals at a limited number of screening dates in a limited number of herds. Even with such a partial information, our method succeeds in estimating many parameters of a spatiotemporal and stochastic epidemiological models with a high accuracy. Data initially available at the individual level become finally more relevant when aggregated at herd scale.

TBC

## Supporting information

**S1 Table.** Performances of 16 candidate objective functions based on an LHS of 2,000 scenarios

**S2 Table.** Numerical identifiability analysis on 20 simulated scenarios (40 simulated datasets).

**S1 Fig.** Comparison the approximate composite log-likelihood considering or neglecting the first-order Markovian dependence.

**S2 Fig.** Comparison of true and estimated initial within-herd prevalence distribution for 20 simulated scenarios (40 simulated datasets).

**S3 Fig.** Assessment of the impact of sub-optimal numerical optimization on the calibration of thresholds to build confidence intervals.

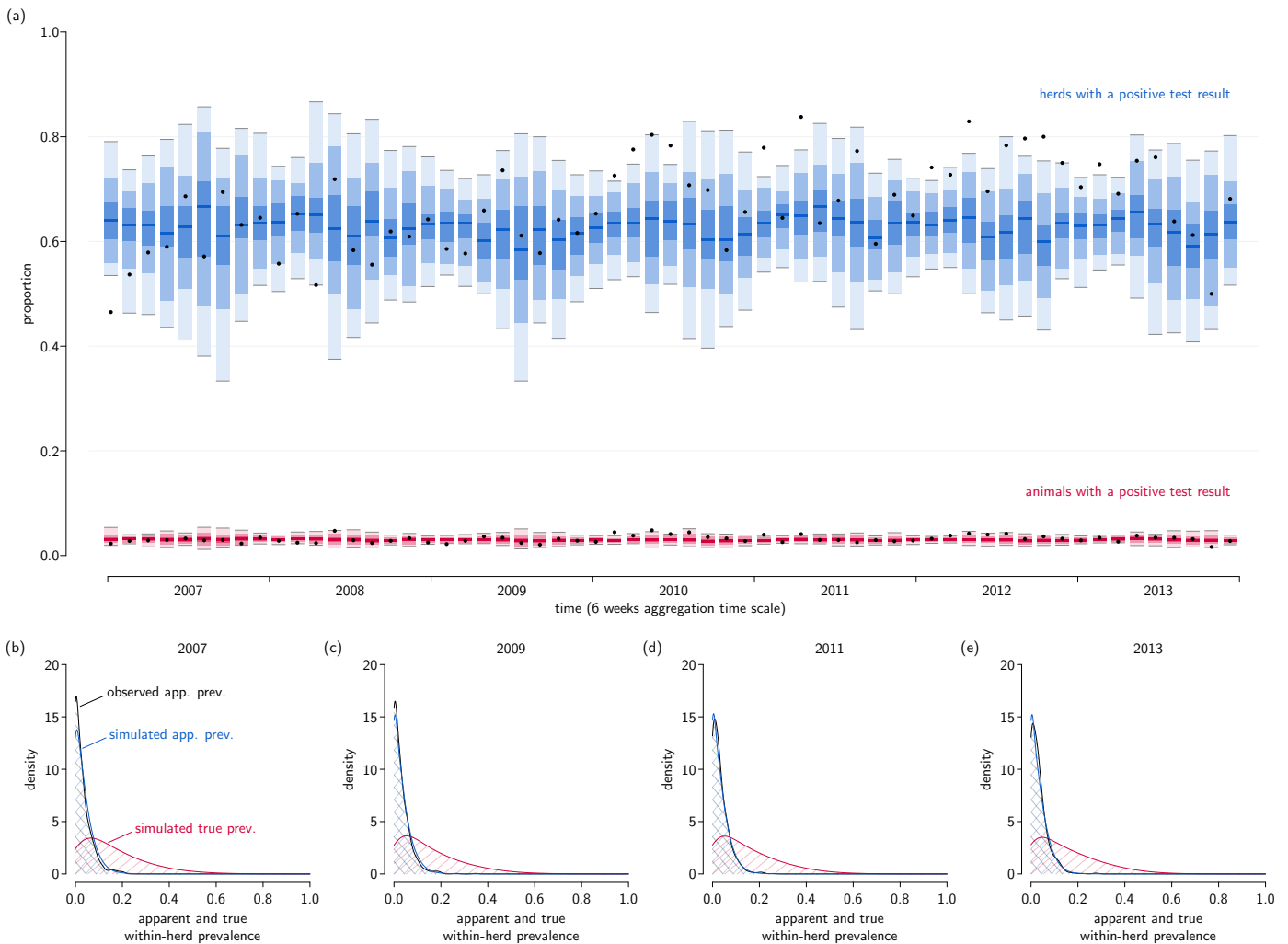


**Fig 8.** Observation versus simulation. (a) proportion of herds (in blue) and animals (in red) with a positive test result. Black points correspond to the observed data. For the simulation, each bar is divided into four levels of color intensity, corresponding, from darkest to lightest, to the median, and to the quantiles 25-75, 5-95 and 0-100, computed from a simulation of 200 runs with the estimated parameter values. (b - e) within-herd prevalence per year. Distributions in black and blue, correspond, respectively, to the observed data and simulated predictions of the apparent within-herd prevalence, and distributions in red correspond to the simulated predictions of the true within-herd prevalence, among the sampled herds, for a given year.

**S4 Fig.** Evolution of the parameter values across iterations of the procedure on real data (runs 1-4).

**S5 Fig.** Evolution of the parameter values through profiles of approximate composite likelihood.

## Acknowledgments

This work was carried out with the financial support of the French Research Agency (ANR), Program Investments for the Future, project ANR-10-BINF-07 (MIHMES),

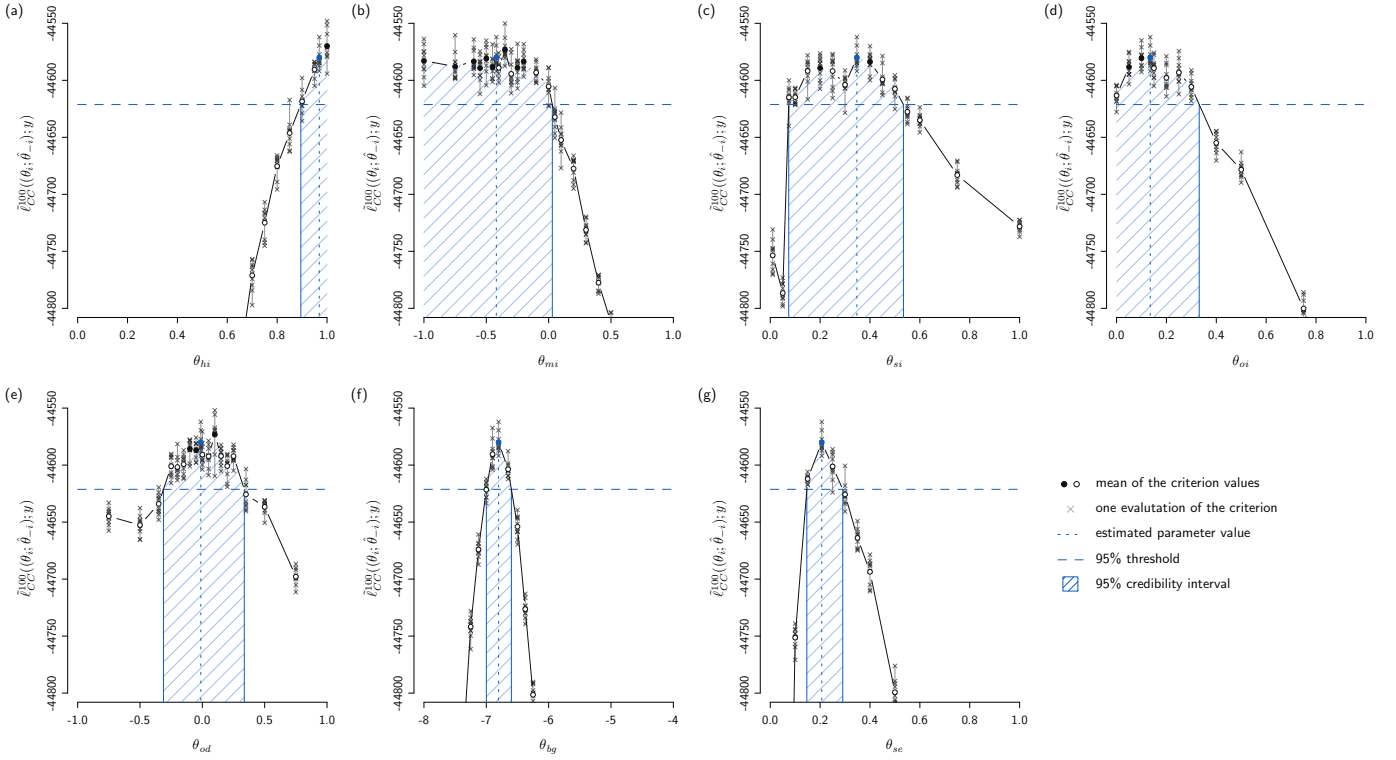


**Fig 9.** Confidence intervals. Profile likelihood were drawn using local estimations by fixing, one at a time, the parameters at different values. The 95% confidence intervals are built using corresponding threshold defined before. With black and white points: black when the distribution of  $\tilde{\ell}_{CC}^{100}(\theta_i; \hat{\theta}_{-i}; y)$  is not statistically different from the 10 evaluations of  $\tilde{\ell}_{CC}^{100}(\hat{\theta}; y)$ , at the 5% significance level as assessed with a t-test, white otherwise.

project ANR-16-CE32-0007-01 (CADENCE), the INRAE Méta-programme GISA, project PREDICATT, and the European Union through the European fund for the regional development (FEDER) of Pays-de-la-Loire. We thank the DGAI and GDS Bretagne for providing the data. We are grateful to the INRAE MIGALE bioinformatics facility (MIGALE, INRAE, 2020. Migale bioinformatics Facility, doi: 10.15454/1.5572390655343293E12) for providing computing resources.

## References

1. Bajardi P, Barrat A, Savini L, Colizza V. Optimizing surveillance for livestock disease spreading through animal movements. *Journal of The Royal Society Interface*. 2012;9(76):2814–2825.
2. Buhnerkempe MG, Tildesley MJ, Lindström T, Gear DA, Portacci K, Miller RS, et al. The impact of movements and animal density on continental scale cattle disease outbreaks in the United States. *PLoS ONE*. 2014;9(3):e91724.
3. Ezanno P, Andraud M, Beaunée G, Hoch T, Krebs S, Rault A, et al. How mechanistic modelling supports decision making for the control of enzootic infectious diseases. *Epidemics*. 2020;32:100398. doi:10.1016/j.epidem.2020.100398.
4. Künzler R, Torgerson P, Keller S, Wittenbrink M, Stephan R, Knubben-Schweizer G, et al. Observed management practices in relation to the

- risk of infection with paratuberculosis and to the spread of *Mycobacterium avium* subsp. *paratuberculosis* in Swiss dairy and beef herds. *BMC Veterinary Research*. 2014;10(1):132. doi:10.1186/1746-6148-10-132.
5. Lindström T, Lewerin SS, Wennergren U. Influence on disease spread dynamics of herd characteristics in a structured livestock industry. *Journal of the Royal Society Interface*. 2012;9(71):1287–1294. doi:10.1098/rsif.2011.0625.
  6. Brooks-Pollock E, Keeling M. Herd size and bovine tuberculosis persistence in cattle farms in Great Britain. *Preventive Veterinary Medicine*. 2009;92(4):360–365.
  7. Stahl K, Lindberg A, Rivera H, Ortiz C, Moreno-Lopez J. Self-clearance from BVDV infections - A frequent finding in dairy herds in an endemically infected region in Peru. *Preventive Veterinary Medicine*. 2008;83(3-4):285–296.
  8. Ezanno P, Fourichon C, Seegers H. Influence of herd structure and type of virus introduction on the spread of bovine viral diarrhoea virus (BVDV) on the spread of bovine viral diarrhoea virus (BVDV) within a dairy herd. *Veterinary Research*. 2008;39(5):39–12.
  9. Marcé C, Ezanno P, Seegers H, Pfeiffer DU, Fourichon C. Within-herd contact structure and transmission of *Mycobacterium avium* subspecies *paratuberculosis* in a persistently infected dairy cattle herd. *Preventive Veterinary Medicine*. 2011;100(2):116–125.
  10. Flaten O, Lien G, Koesling M, Valle PS, Ebbesvik M. Comparing risk perceptions and risk management in organic and conventional dairy farming: empirical results from Norway. *Livestock Production Science*. 2005;95(1-2):11–25.
  11. Ersbøll AK, Ersbøll BK, Houe H, Alban L, Kjeldsen AM. Spatial modelling of the between-herd infection dynamics of bovine virus diarrhoea virus (BVDV) in dairy herds in Denmark. *Preventive Veterinary Medicine*. 2010;97(2):83–89.
  12. Dutta BL, Ezanno P, Vergu E. Characteristics of the spatio-temporal network of cattle movements in France over a 5-year period. *Preventive Veterinary Medicine*. 2014;117(1):79–94.
  13. Beaunée G, Vergu E, Ezanno P. Modelling of paratuberculosis spread between dairy cattle farms at a regional scale. *Veterinary Research*. 2015;46(1):295.
  14. Qi L, Beaunée G, Arnoux S, Dutta BL, Joly A, Vergu E, et al. Neighbourhood contacts and trade movements drive the regional spread of bovine viral diarrhoea virus (BVDV). *Veterinary Research*. 2019;50(1):30. doi:10.1186/s13567-019-0647-x.
  15. Beaumont MA, Zhang W, Balding DJ. Approximate Bayesian computation in population genetics. *Genetics*. 2002;162(4):2025–2035.
  16. Toni T, Welch D, Strelkova N, Ipsen A, Stumpf MPH. Approximate Bayesian computation scheme for parameter inference and model selection in dynamical systems. *Journal of the Royal Society, Interface*. 2009;6(31):187–202.
  17. Ster IC, Singh BK, Ferguson NM. Epidemiological inference for partially observed epidemics: The example of the 2001 foot and mouth epidemic in Great Britain. *Epidemics*. 2009;1(1):21 – 34. doi:https://doi.org/10.1016/j.epidem.2008.09.001.

18. Brooks-Pollock E, Roberts GO, Keeling MJ. A dynamic model of bovine tuberculosis spread and control in Great Britain. *Nature*. 2014;511(7508):228–231.
19. Behr MA, Collins DM. Paratuberculosis: organism, disease, control. CAB International, Cambridge. 2010;.
20. Ott SL, Wells SJ, Wagner BA. Herd-level economic losses associated with Johne's disease on US dairy operations. *Preventive Veterinary Medicine*. 1999;40(3-4):179–192.
21. Lombard JE, Garry FB, Garry FB, McCluskey BJ, McCluskey BJ, Wagner BA, et al. Risk of removal and effects on milk production associated with paratuberculosis status in dairy cows. *Journal of the American Veterinary Medical Association*. 2005;227(12):1975–1981.
22. Garcia AB, Shalloo L. Invited review: The economic impact and control of paratuberculosis in cattle. *Journal of Dairy Science*. 2015;98(8):1–21.
23. Marcé C, Ezanno P, Weber MF, Seegers H, Pfeiffer DU, Fourichon C. Invited review: Modeling within-herd transmission of *Mycobacterium avium* subspecies paratuberculosis in dairy cattle: A review. *Journal of Dairy Science*. 2010;93(10):4455–4470.
24. Beaunée G, Vergu E, Joly A, Ezanno P. Controlling bovine paratuberculosis at a regional scale: Towards a decision modelling tool. *Journal of theoretical biology*. 2017;435:157–183.
25. Nielsen SS, Ersbøll AK. Age at Occurrence of *Mycobacterium avium* Subspecies paratuberculosis in Naturally Infected Dairy Cows. *Journal of Dairy Science*. 2006;89(12):4557–4566.
26. Mitchell RM, Schukken Y, Koets A, Weber M, Bakker D, Stabel J, et al. Differences in intermittent and continuous fecal shedding patterns between natural and experimental *Mycobacterium avium* subspecies paratuberculosis infections in cattle. *Veterinary Research*. 2015;46(1):66.
27. Hagan WA. Age as a Factor in Susceptibility to Johne's Disease. *Cornell Veterinarian*. 1938;28:34–40.
28. Windsor PA, Whittington RJ. Evidence for age susceptibility of cattle to Johne's disease. *The Veterinary Journal*. 2010;184(1):37–44.
29. Nelder JA, Mead R. A simplex method for function minimization. *The computer journal*. 1965;7(4):308–313.
30. Barton RR, Ivey JS Jr. Modifications of the Nelder-Mead Simplex Method for Stochastic Simulation Response Optimization. In: *Proceedings of the 23rd Conference on Winter Simulation. WSC '91. Washington, DC, USA: IEEE Computer Society; 1991. p. 945–953. Available from: <http://dl.acm.org/citation.cfm?id=304238.304373>.*
31. Venzon D, Moolgavkar S. A method for computing profile-likelihood-based confidence intervals. *Journal of the Royal Statistical Society: Series C (Applied Statistics)*. 1988;37(1):87–94.
32. Nielsen SS, Toft N. Ante mortem diagnosis of paratuberculosis: a review of accuracies of ELISA, interferon-gamma assay and faecal culture techniques. *Veterinary Microbiology*. 2008;129(3-4):217–235.

**S1 Table.** Performances of 16 candidate objective functions based on an LHS of 2,000 scenarios

Perf. <sup>a</sup>	Objective function <sup>b</sup>															
	$\tilde{f}_{ASAD}^{100}$	$\tilde{f}_{ASADe}^{100}$	$\tilde{f}_{ASADc}^{100}$	$\tilde{f}_{ASADec}^{100}$	$\tilde{f}_{ASSD}^{100}$	$\tilde{f}_{ASSDe}^{100}$	$\tilde{f}_{ASSDc}^{100}$	$\tilde{f}_{ASSDec}^{100}$	$\tilde{f}_{SSDA}^{100}$	$\tilde{f}_{SSDAe}^{100}$	$\tilde{f}_{SSDAc}^{100}$	$\tilde{f}_{SSDAec}^{100}$	$\tilde{t}_{BI}^{100}$	$\tilde{t}_{MC}^{100}$	$\tilde{t}_{CC}^{100}$	
Rank of $\theta^0$																
first	0.195	0.270	0.355	0.395	0.170	0.400	0.265	0.470	0.897	0.904	0.594	0.598	0.754	0.758	0.970	0.954
top 5%	0.416	0.484	0.467	0.526	0.369	0.452	0.431	0.483	1.00	1.00	0.994	0.994	1.00	1.00	1.00	1.00
Error on parameter ( $ \theta^* - \theta^0 / \theta^{\max} - \theta^{\min} $ )																
$\theta_{hi}$	0.268	0.251	0.270	0.256	0.285	0.305	0.256	0.269	0.019	0.018	0.054	0.054	0.034	0.033	0.001	0.002
$\theta_{mi}$	0.260	0.263	0.264	0.264	0.259	0.272	0.257	0.267	0.027	0.025	0.115	0.117	0.072	0.071	0.006	0.011
$\theta_{si}$	0.328	0.320	0.325	0.317	0.352	0.339	0.347	0.335	0.027	0.025	0.121	0.120	0.069	0.067	0.006	0.009
$\theta_{mit}$	0.214	0.209	0.214	0.214	0.206	0.206	0.209	0.212	0.017	0.015	0.073	0.074	0.043	0.042	0.004	0.006
$\theta_{sit}$	0.264	0.254	0.260	0.254	0.278	0.263	0.279	0.270	0.019	0.018	0.088	0.088	0.048	0.048	0.004	0.007
$\theta_{oi}$	0.253	0.270	0.246	0.253	0.278	0.288	0.278	0.287	0.015	0.015	0.068	0.067	0.040	0.038	0.004	0.005
$\theta_{od}$	0.240	0.244	0.219	0.220	0.254	0.267	0.238	0.248	0.016	0.015	0.064	0.062	0.039	0.038	0.005	0.007
$\theta_{bg}$	0.135	0.140	0.129	0.131	0.146	0.165	0.142	0.157	0.008	0.007	0.040	0.041	0.023	0.022	0.002	0.003
$\theta_{se}$	0.157	0.168	0.141	0.148	0.196	0.214	0.175	0.191	0.012	0.011	0.028	0.028	0.022	0.023	0.002	0.003
Error on parameter, after excluding the true scenario ( $ \theta^+ - \theta^0 / \theta^{\max} - \theta^{\min} $ )																
$\theta_{hi}$	0.269	0.253	0.272	0.261	0.287	0.311	0.261	0.276	0.157	0.157	0.155	0.154	0.152	0.152	0.080	0.085
$\theta_{mi}$	0.263	0.267	0.271	0.272	0.262	0.281	0.261	0.277	0.276	0.278	0.280	0.280	0.282	0.283	0.246	0.245
$\theta_{si}$	0.334	0.328	0.335	0.328	0.358	0.351	0.355	0.348	0.288	0.287	0.296	0.298	0.299	0.300	0.257	0.253
$\theta_{mit}$	0.217	0.214	0.221	0.222	0.209	0.215	0.214	0.222	0.171	0.172	0.186	0.186	0.173	0.175	0.143	0.139
$\theta_{sit}$	0.269	0.261	0.268	0.264	0.283	0.273	0.286	0.280	0.211	0.211	0.224	0.225	0.216	0.217	0.174	0.170
$\theta_{oi}$	0.257	0.276	0.254	0.263	0.281	0.299	0.283	0.298	0.166	0.167	0.167	0.168	0.173	0.176	0.148	0.148
$\theta_{od}$	0.245	0.251	0.227	0.231	0.258	0.278	0.246	0.262	0.177	0.179	0.165	0.165	0.178	0.180	0.175	0.171
$\theta_{bg}$	0.137	0.144	0.133	0.136	0.148	0.170	0.145	0.164	0.076	0.077	0.086	0.087	0.084	0.085	0.081	0.077
$\theta_{se}$	0.159	0.170	0.144	0.151	0.197	0.216	0.178	0.194	0.083	0.083	0.077	0.078	0.082	0.083	0.059	0.057

<sup>a</sup> See Table 2 for a definition of the different performance measures. <sup>b</sup> Objective functions: *ASAD*, average sum of absolute differences between the proportion of positive tests; *ASSD*, the average sum of squared differences between the proportion of positive tests; *SSDA*, sum of squared differences between the average proportion of positive tests; *BI*, log-likelihood under a binomial model with independent sampling events; *MC*, marginal composite likelihood; *CC*, conditional composite likelihood. As described in the Methods section, the subscripts *e* and *c* denote variants of these objective functions: *e*, proportion of positive tests in each simulated trajectory is replaced by its expected value; *c*, reweighing each term of the objective function by the square of the number of tests. Values for *ASSD*, *SSDA*, *BI*, *MC*, and *CC* are the same as those reported in Table 2.

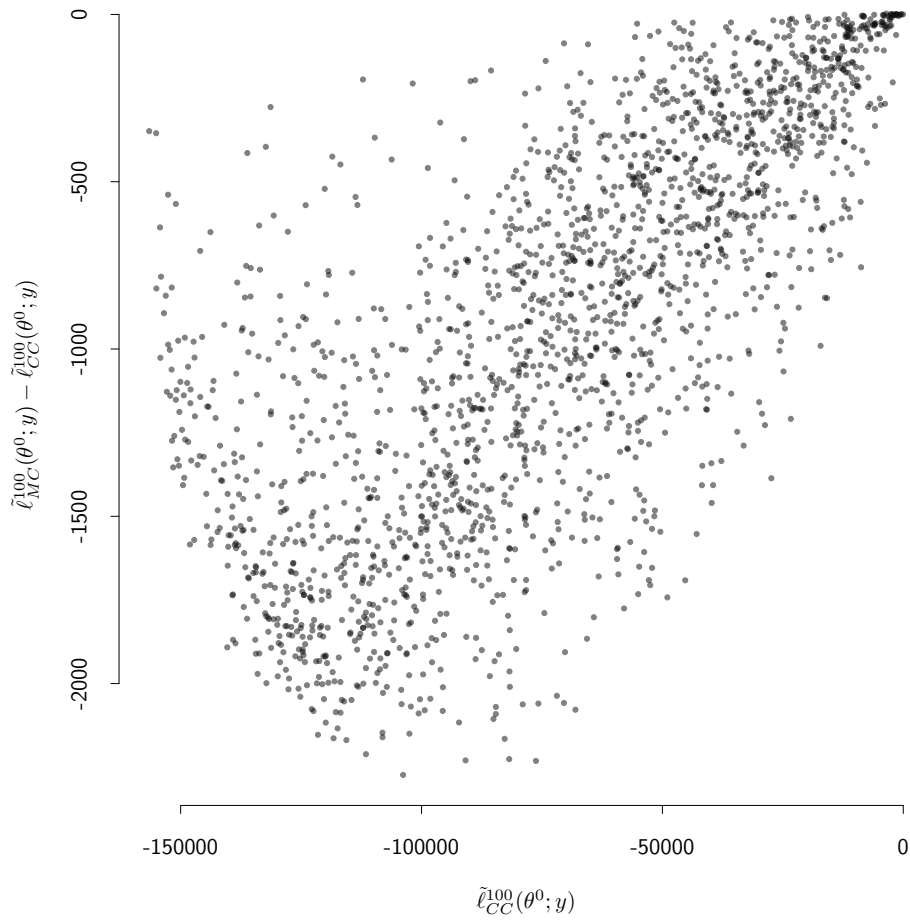
**S2 Table.** Numerical identifiability analysis on 20 simulated scenarios (40 simulated datasets).

#	True and estimated parameter values														Objective function		t-test <sup>a</sup>
	$\theta_{hi}^o$	$\theta_{hi}^*$	$\theta_{mit}^o$	$\theta_{mit}^*$	$\theta_{sit}^o$	$\theta_{sit}^*$	$\theta_{oi}^o$	$\theta_{oi}^*$	$\theta_{od}^o$	$\theta_{od}^*$	$\theta_{bq}^o$	$\theta_{bq}^*$	$\theta_{se}^o$	$\theta_{se}^*$	$\bar{\ell}_{CC}^{100}(\theta^0; y)$	$\bar{\ell}_{CC}^{100}(\hat{\theta}; y)$	p-value
1a	0.87	0.87	0.22	0.29	0.18	0.22	0.33	0.38	0.00	-0.00	-7.10	-7.19	0.94	0.80	-83 646.0	-83 593.9	-
1b	0.87	0.85	0.22	0.33	0.18	0.23	0.33	0.39	0.00	-0.02	-7.10	-7.27	0.94	0.76	-83 619.2	-83 572.7	-
2a	0.11	0.14	0.15	0.24	0.13	0.19	0.46	0.48	-0.17	-0.07	-6.21	-6.25	0.55	0.48	-47 044.6	-46 996.6	-
2b	0.11	0.14	0.15	0.31	0.13	0.22	0.46	0.48	-0.17	-0.14	-6.21	-6.29	0.55	0.49	-46 155.0	-46 173.7	0.078
3a	0.49	0.61	0.10	0.09	0.08	0.08	0.74	0.60	0.20	0.30	-4.56	-5.23	0.05	0.06	-28 140.9	-28 144.7	0.065
3b	0.49	0.48	0.10	0.15	0.08	0.13	0.74	0.87	0.20	-0.12	-4.56	-5.25	0.05	0.06	-28 284.0	-28 291.1	3.6e-03 <sup>b</sup>
4a	0.91	0.84	0.05	0.07	0.04	0.07	0.39	0.59	0.31	0.12	-6.84	-6.83	0.35	0.28	-42 249.9	-42 239.5	-
4b	0.91	0.71	0.05	0.10	0.04	0.08	0.39	0.56	0.31	0.35	-6.84	-6.88	0.35	0.25	-41 380.4	-41 376.5	-
5a	0.58	0.61	0.08	0.12	0.06	0.10	0.15	0.17	-0.38	-0.45	-6.50	-6.50	0.46	0.33	-35 280.7	-35 273.7	-
5b	0.58	0.60	0.08	0.13	0.06	0.11	0.15	0.18	-0.38	-0.39	-6.50	-6.58	0.46	0.34	-36 203.3	-36 192.0	-
6a	0.18	0.23	0.13	0.13	0.08	0.12	0.65	0.84	0.47	0.22	-5.90	-5.95	0.74	0.67	-81 869.0	-81 838.5	-
6b	0.18	0.21	0.13	0.21	0.08	0.17	0.65	0.82	0.47	0.22	-5.90	-5.98	0.74	0.70	-81 787.5	-81 791.4	0.84
7a	0.69	0.72	0.20	0.20	0.05	0.15	0.56	0.56	-0.09	-0.05	-5.47	-5.18	0.68	0.63	-136 112.1	-136 224.4	5.6e-12
7b	0.69	0.76	0.20	0.20	0.05	0.14	0.56	0.58	-0.09	-0.02	-5.47	-5.24	0.68	0.63	-136 887.9	-137 010.4	2.2e-11
8a	0.37	0.41	0.30	0.40	0.10	0.25	0.05	0.06	-0.21	-0.44	-4.84	-4.86	0.28	0.28	-59 054.5	-59 102.5	8.4e-10
8b	0.37	0.41	0.30	0.35	0.10	0.23	0.05	0.03	-0.21	-0.16	-4.84	-5.00	0.28	0.28	-60 234.7	-60 267.9	2.1e-04
9a	0.29	0.38	0.40	0.34	0.15	0.23	0.89	0.90	0.29	0.40	-7.35	-7.36	0.83	0.82	-73 143.6	-73 196.3	9.5e-07
9b	0.29	0.37	0.40	0.37	0.15	0.24	0.89	0.94	0.29	0.37	-7.35	-7.39	0.83	0.80	-73 216.9	-73 251.7	1.7e-04
10a	0.71	0.74	0.31	0.37	0.21	0.24	0.19	0.16	-0.43	-0.26	-5.11	-5.16	0.22	0.21	-81 253.8	-81 254.1	0.97
10b	0.71	0.75	0.31	0.26	0.21	0.19	0.19	0.13	-0.43	-0.24	-5.11	-5.13	0.22	0.22	-81 425.1	-81 425.9	0.80
11a	0.88	0.92	0.05	0.05	0.05	0.05	0.03	0.02	-0.45	-0.19	-5.83	-5.83	0.39	0.38	-62 359.3	-62 342.8	-
11b	0.88	0.81	0.05	0.07	0.05	0.06	0.03	0.00	-0.45	0.03	-5.83	-5.81	0.39	0.35	-60 199.2	-60 184.7	-
12a	0.14	0.15	0.21	0.35	0.17	0.23	0.16	0.18	0.05	0.04	-6.11	-6.08	0.26	0.21	-25 199.1	-25 198.4	-
12b	0.14	0.15	0.21	0.35	0.17	0.23	0.16	0.18	0.05	0.04	-6.11	-6.18	0.26	0.23	-26 313.7	-26 292.4	-
13a	0.59	0.62	0.33	0.33	0.22	0.23	0.82	0.88	0.32	0.15	-4.98	-5.13	0.62	0.62	-129 600.9	-129 587.4	-
13b	0.59	0.59	0.33	0.35	0.22	0.24	0.82	0.88	0.32	0.28	-4.98	-5.01	0.62	0.61	-129 417.4	-129 403.8	-
14a	0.30	0.31	0.38	0.37	0.04	0.20	0.70	0.72	-0.25	-0.25	-4.54	-4.30	0.15	0.15	-54 441.6	-54 456.5	4.9e-04
14b	0.30	0.32	0.38	0.37	0.04	0.24	0.70	0.69	-0.25	-0.12	-4.54	-4.57	0.15	0.15	-53 050.9	-53 065.8	1.9e-04
15a	0.61	0.63	0.37	0.37	0.24	0.24	0.20	0.25	0.14	0.09	-5.52	-5.55	0.50	0.49	-111 653.4	-111 649.2	-
15b	0.61	0.61	0.37	0.36	0.24	0.24	0.20	0.24	0.14	0.06	-5.52	-5.44	0.50	0.49	-110 144.8	-110 143.5	-
16a	0.33	0.37	0.04	0.04	0.04	0.04	0.76	0.90	0.43	-0.04	-6.31	-6.39	0.07	0.07	-17 779.5	-17 783.8	0.047
16b	0.33	0.24	0.04	0.07	0.04	0.06	0.76	0.93	0.43	0.11	-6.31	-6.46	0.07	0.07	-17 559.8	-17 565.2	0.015
17a	0.76	0.77	0.15	0.13	0.12	0.11	0.30	0.37	0.26	0.17	-5.11	-5.03	0.83	0.82	-130 882.6	-130 876.9	-
17b	0.76	0.81	0.15	0.15	0.12	0.12	0.30	0.46	0.26	0.01	-5.11	-5.29	0.83	0.82	-132 446.7	-132 430.8	-
18a	0.96	0.84	0.03	0.05	0.03	0.04	0.53	0.67	-0.38	-0.37	-7.45	-7.44	0.43	0.30	-24 823.9	-24 793.3	-
18b	0.96	0.67	0.03	0.08	0.03	0.07	0.53	0.85	-0.38	-0.55	-7.45	-7.66	0.43	0.24	-23 486.6	-23 472.8	-
19a	0.45	0.46	0.51	0.51	0.21	0.24	0.39	0.43	-0.02	0.04	-6.78	-6.76	0.86	0.78	-88 332.4	-88 304.6	-
19b	0.45	0.50	0.51	0.44	0.21	0.25	0.39	0.47	-0.02	-0.10	-6.78	-6.75	0.86	0.80	-91 585.6	-91 583.8	-
20a	0.01	0.03	0.37	0.33	0.22	0.23	0.61	0.78	-0.17	-0.21	-7.10	-7.23	0.73	0.58	-36 395.3	-36 347.8	-
20b	0.01	0.04	0.37	0.27	0.22	0.21	0.61	0.72	-0.17	-0.05	-7.10	-7.10	0.73	0.54	-36 581.6	-36 392.5	-

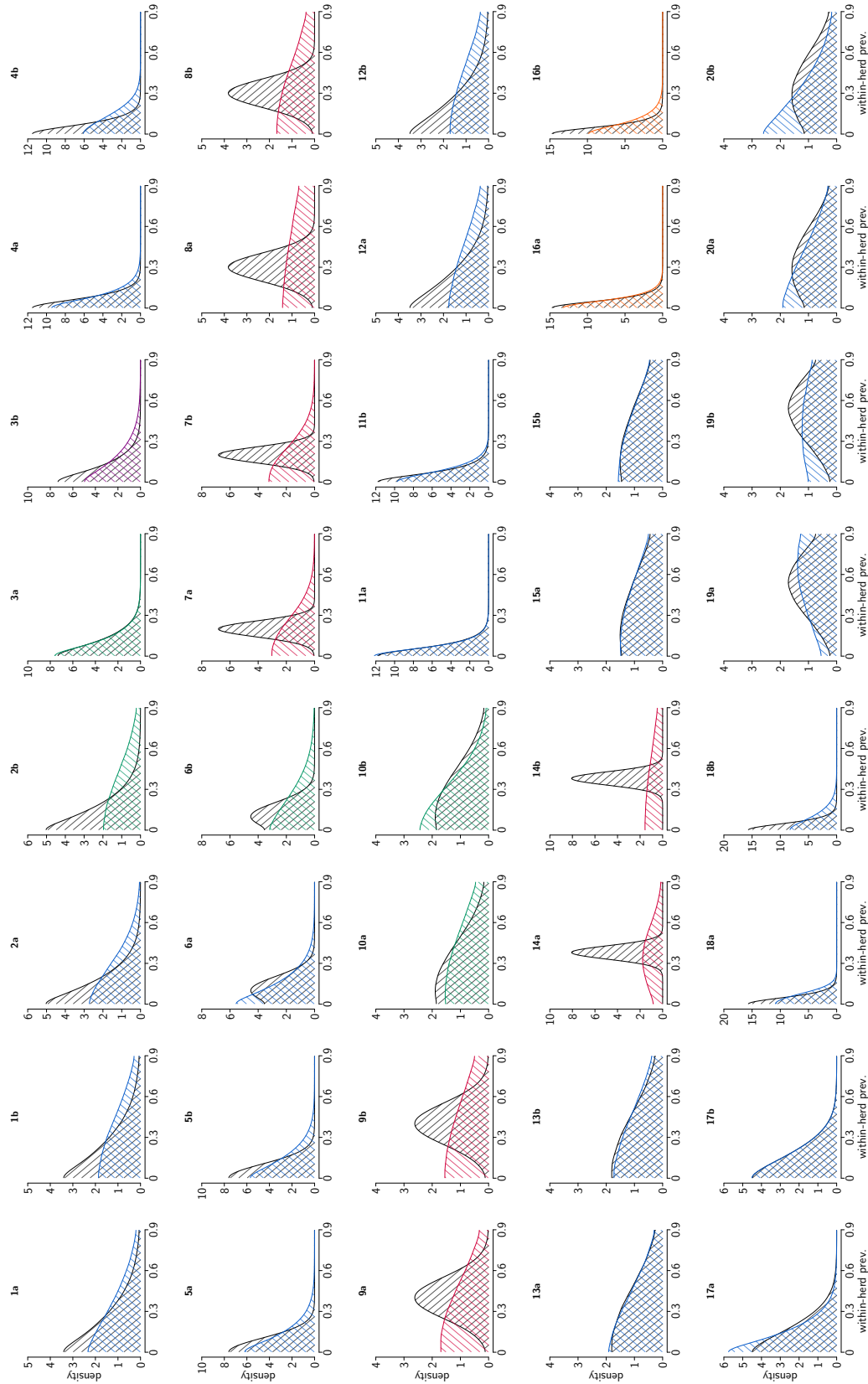
<sup>a</sup> t-test comparing the 10 evaluations of  $\bar{\ell}_{CC}^{100}(\theta; y)$  used to compute  $\bar{\ell}_{CC}^{100}(\hat{\theta}; y)$  for each  $\theta$ , when  $\bar{\ell}_{CC}^{100}(\hat{\theta}; y) < \bar{\ell}_{CC}^{100}(\theta^0; y)$ .

<sup>b</sup> Particular case for scenario 3b where  $\bar{\ell}_{CC}^{100}(\theta^0; y) > \bar{\ell}_{CC}^{100}(\hat{\theta}; y)$ , but  $\max(\bar{\ell}_{CC}^{100}(\theta^0; y)) < \max(\bar{\ell}_{CC}^{100}(\hat{\theta}; y))$ , considering all evaluation of the objective function for  $\hat{\theta}$  (the value obtain during the optimisation process and the 10 additional evaluations of  $\bar{\ell}_{CC}^{100}(\hat{\theta}; y)$ ).

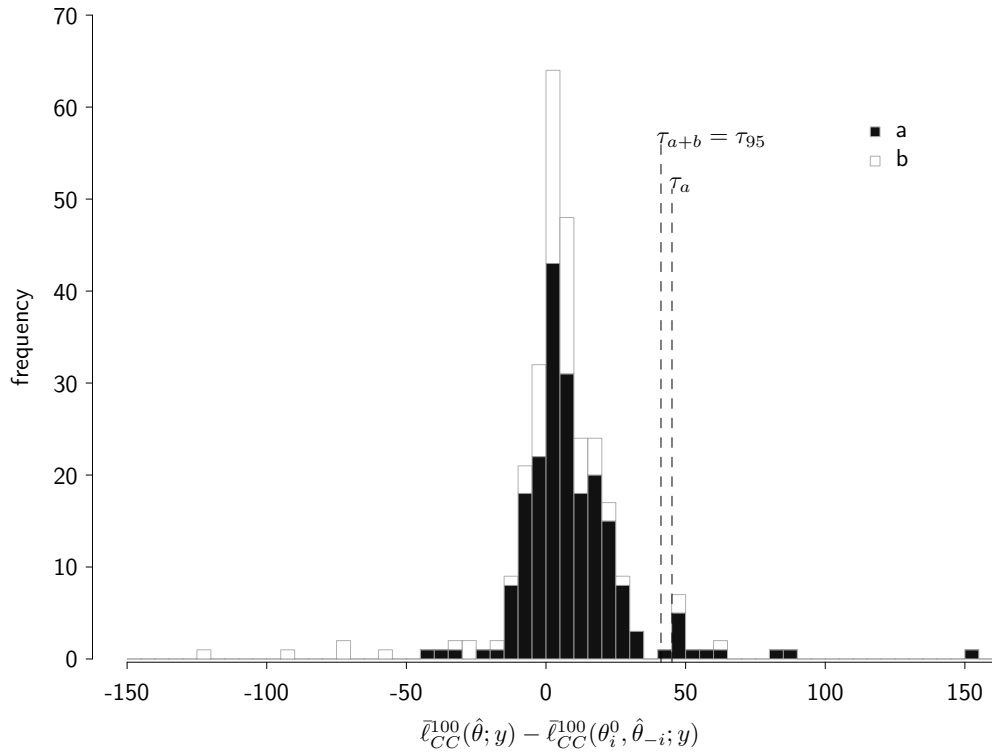




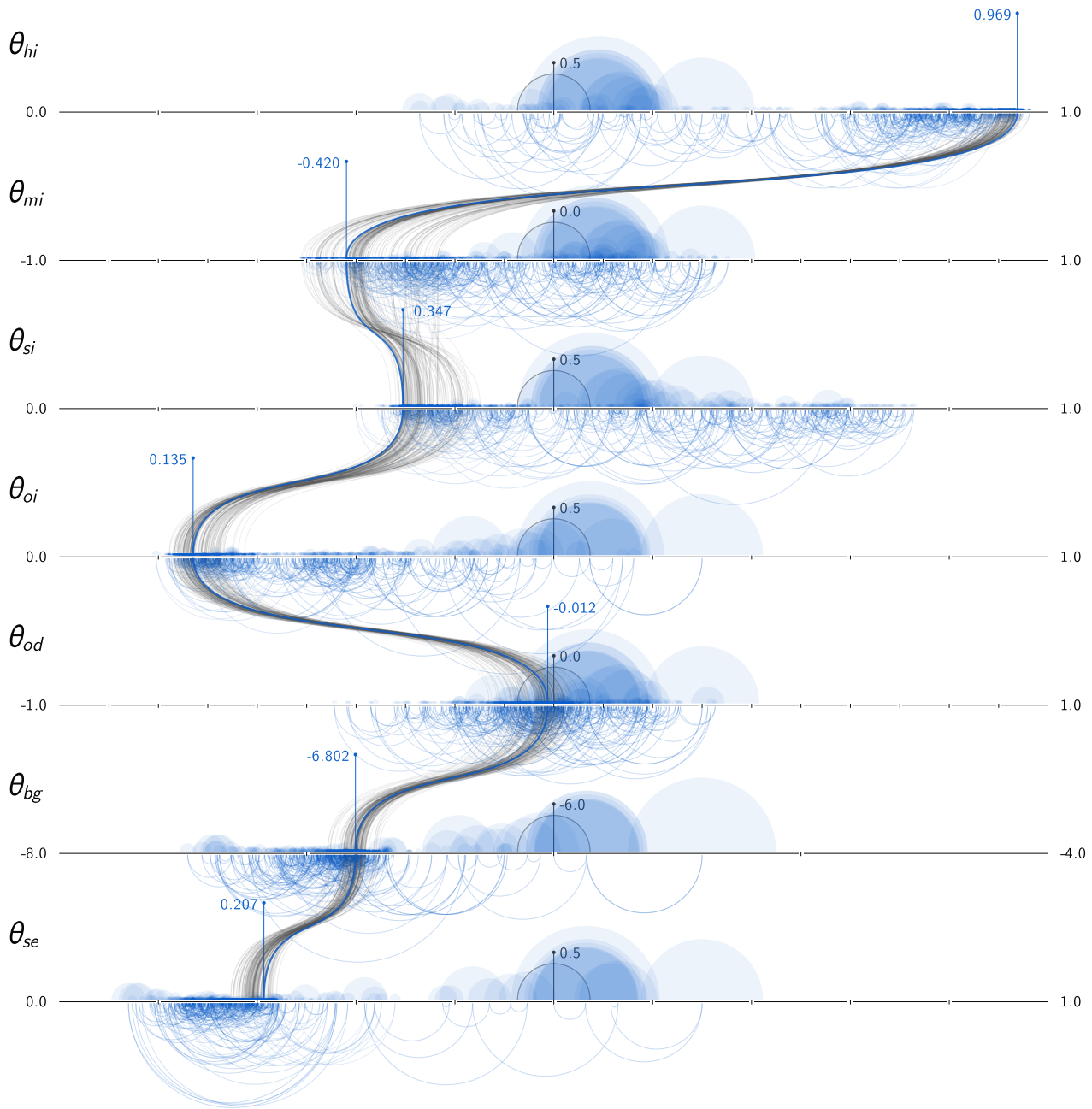
**S1 Fig.** Comparison the approximate composite log-likelihood considering or neglecting the first-order Markovian dependence. Dependence between consecutive sampling points is taken into account in  $\ell_{CC}(\theta; y)$  but not in  $\ell_{MC}(\theta; y)$ .



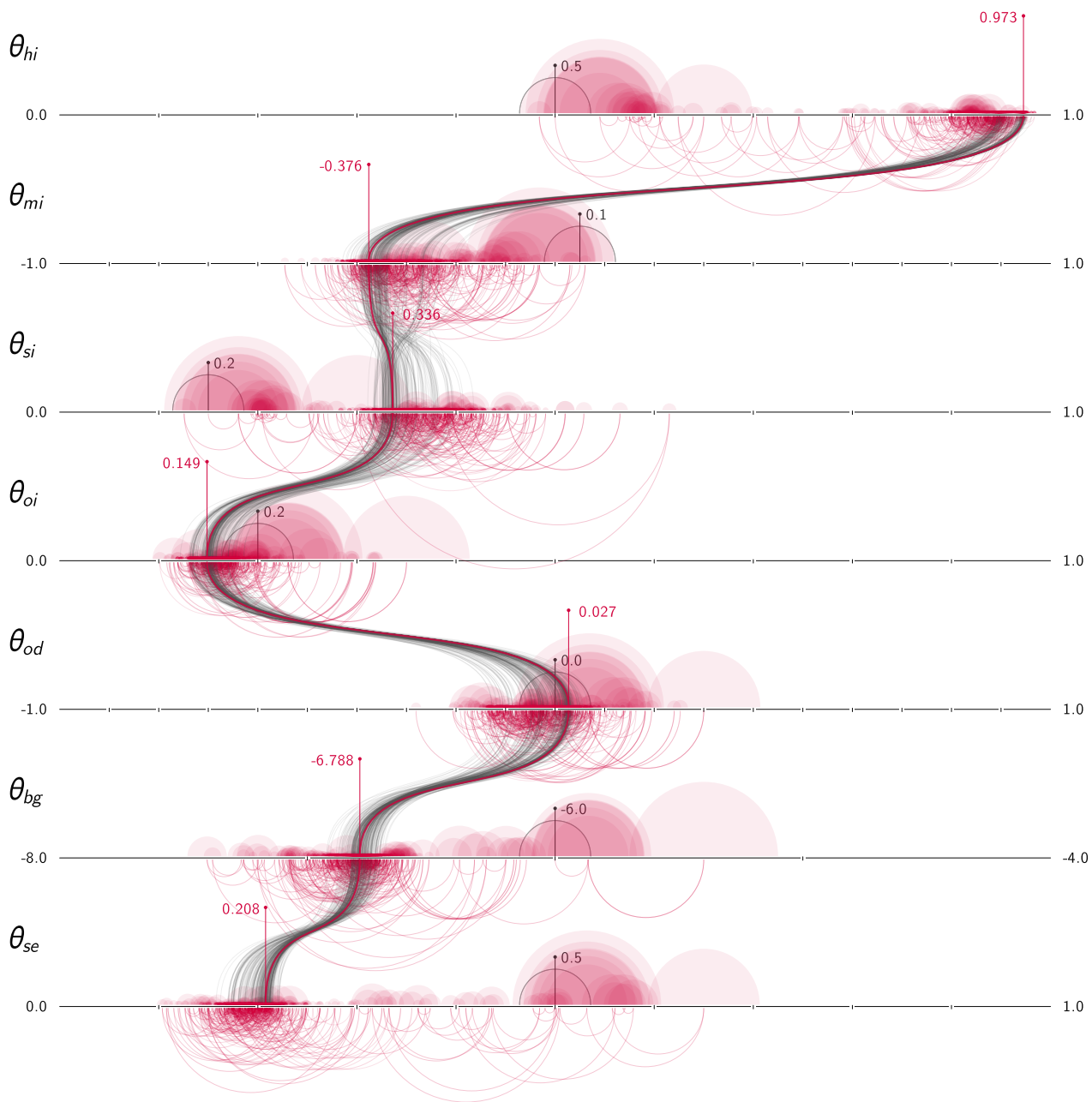
**S2 Fig.** Comparison of true and estimated initial within-herd prevalence distribution for 20 simulated scenarios (40 simulated datasets). (color: blue when  $\bar{\ell}_{CC}^{100}(\theta; y) > \bar{\ell}_{CC}^{100}(\theta^0; y)$ , green or yellow when the difference is not statistically different, respectively, at the 5% or 1% significance level as assessed with a t-test comparing the 10 evaluations of  $\bar{\ell}_{CC}^{100}(\theta; y)$  used to compute  $\bar{\ell}_{CC}^{100}(\theta; y)$  for each  $\theta$ , red otherwise, except for scenario 3b in purple for the reason mention in S2 Table).



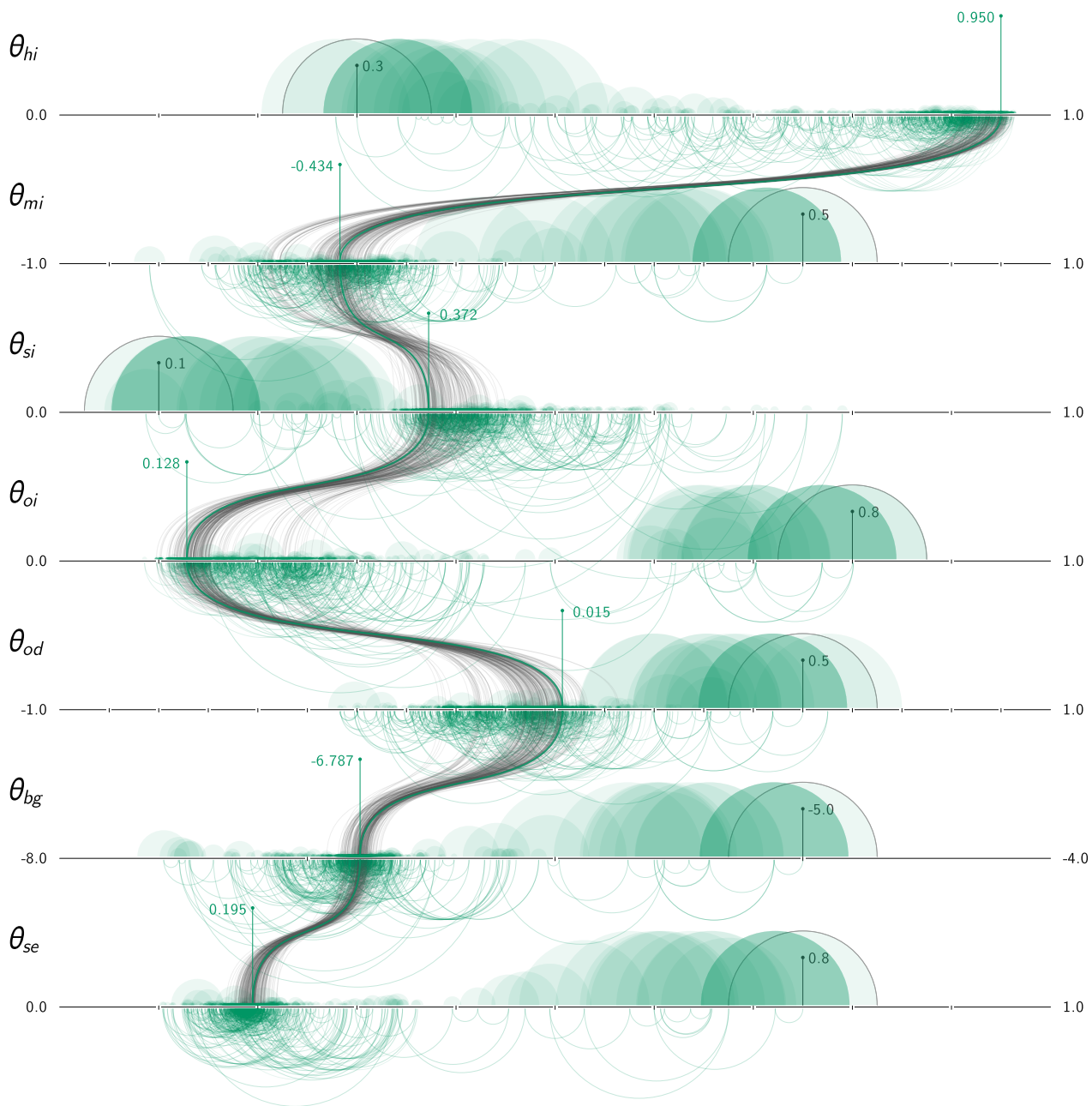
**S3 Fig.** Assessment of the impact of sub-optimal numerical optimization on the calibration of thresholds to build confidence intervals. The empirical distribution of  $\bar{\ell}_{CC}^{100}(\hat{\theta}; y) - \bar{\ell}_{CC}^{100}(\theta_i^0, \hat{\theta}_{-i}; y)$  that served to calibrate the thresholds is represented. Black and white areas distinguish datasets according to the sign of  $\bar{\ell}_{CC}^{100}(\hat{\theta}; y) - \bar{\ell}_{CC}^{100}(\theta^0; y)$ : black when positive or when the distribution of  $\bar{\ell}_{CC}^{100}(\hat{\theta}; y)$  is not statistically different from the 10 evaluations of  $\bar{\ell}_{CC}^{100}(\theta^0; y)$ , at the 5% significance level as assessed with a t-test, white otherwise (see Fig. 6). Quantiles at level 95% of the total distribution and of the distribution excluding white areas are reported.



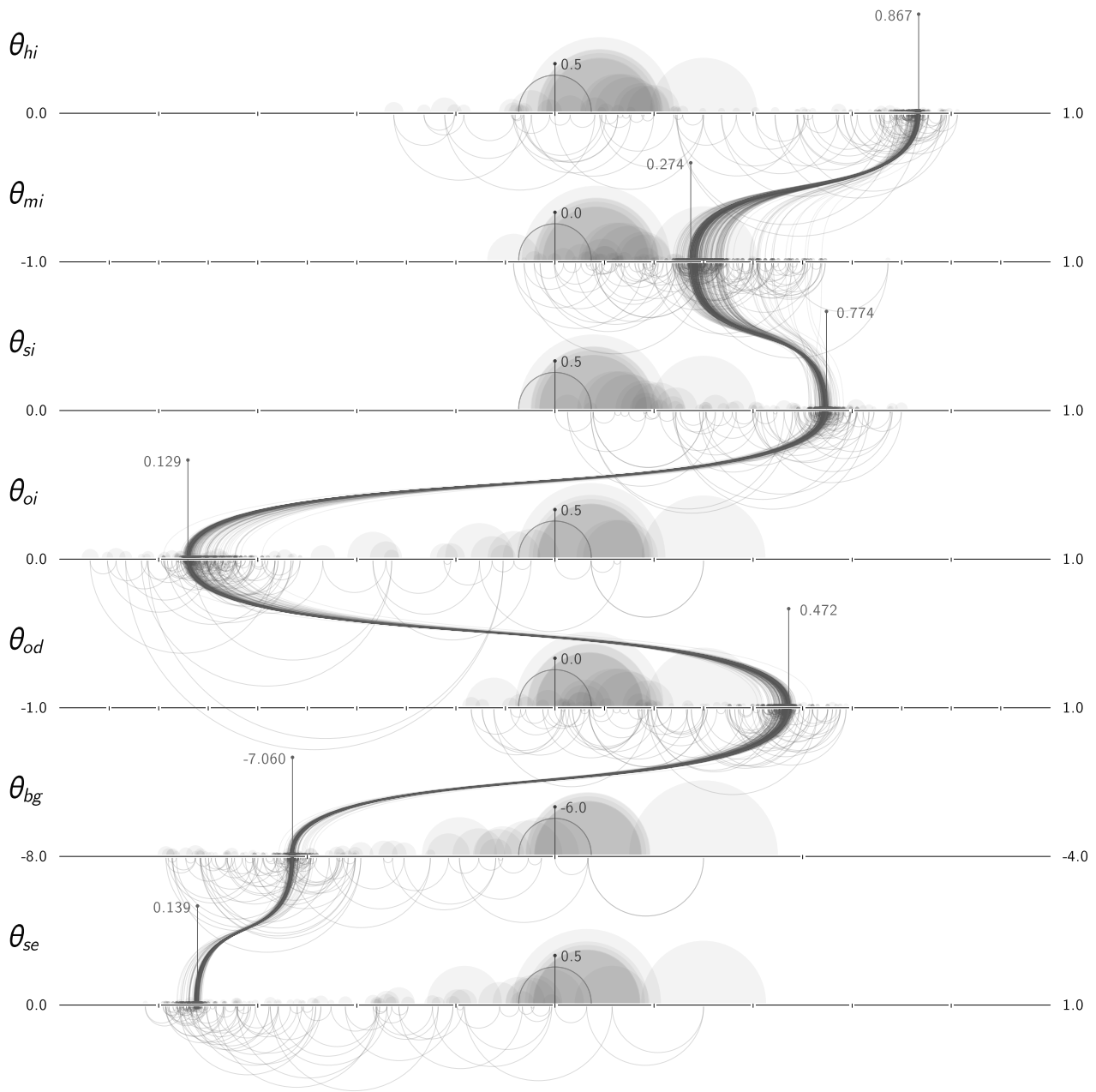
**S4 Fig. (part 1/4)** Run 1 of numerical optimization on real data. Evolution of the parameter values across iterations of the procedure. The half colored discs (above the x-axis) correspond to the quality of the estimation with a size proportional to the distance from the best trajectory (the smaller the radius, the better the value of the criterion). The half discs with border colored in gray correspond to the initial values (reported) used for the estimation. The arcs (below the x-axis) link successive evaluations. The values of the parameters associated with the highest value of the objective function are reported, and highlighted using a thicker colored line. The gray curved lines link the values of the 7 parameters associated with evaluations of the objective function above  $\bar{\ell}_{CC}^{100}(\hat{\theta}; y) - 50$ .



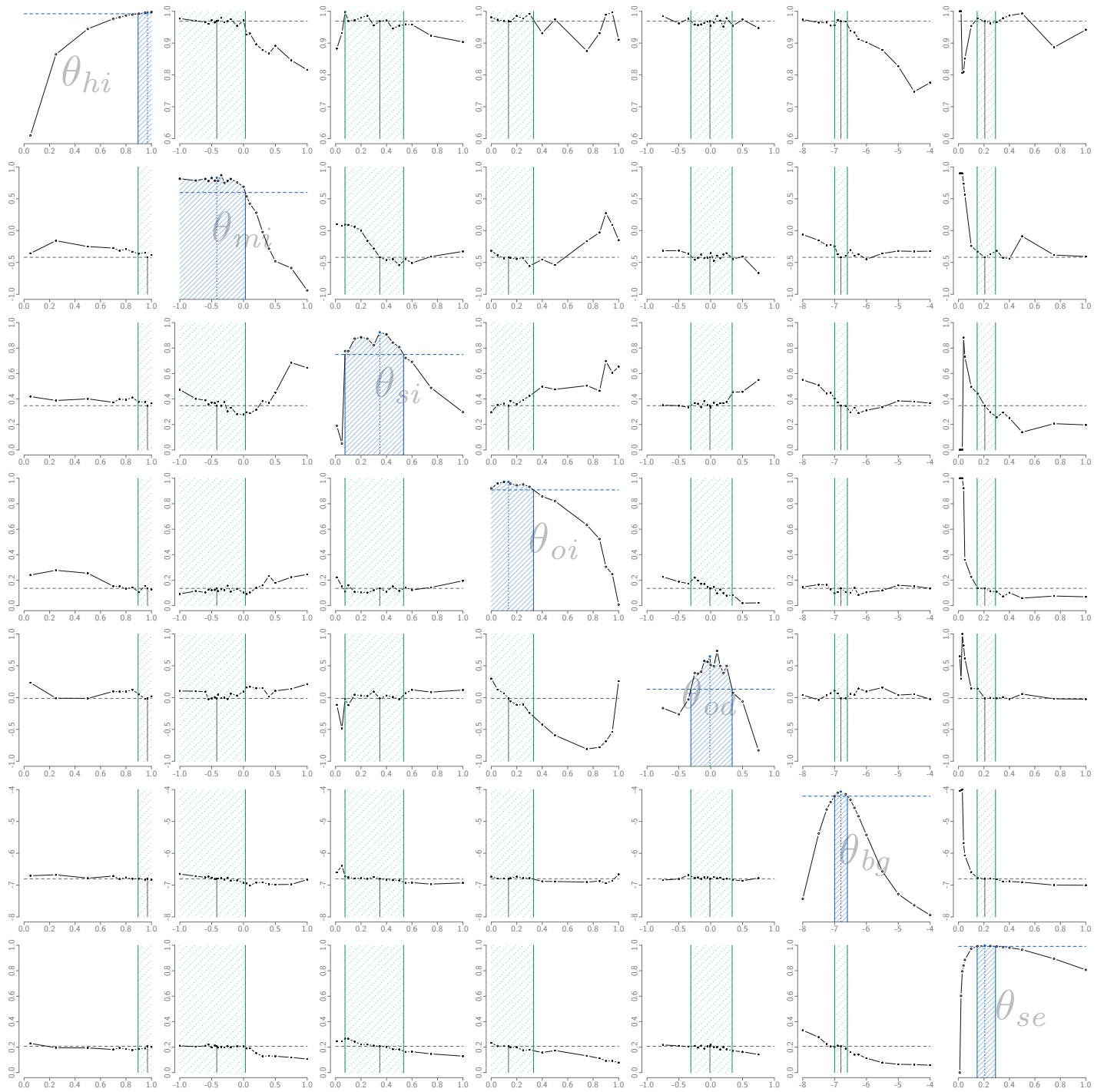
**S4 Fig. (part 2/4)** Run 2 of numerical optimization on real data. Legend on page 28.



**S4 Fig. (part 3/4)** Run 3 of numerical optimization on real data. Legend on page 28.



**S4 Fig. (part 4/4)** Run 4 of numerical optimization on real data. Legend on page 28.



**S5 Fig.** Evolution of the parameter values through profiles of approximate composite likelihood. Building the profiles used to establish confidence intervals for a parameter of interest involved numerical optimization over six other parameters at each point of a grid. The values obtained for these parameters are reported here.